KAOLIN-BASED ADSORBENT FOR ENVIRONMENTAL APPLICATIONS

Submitted in fulfillment of the requirements for the degree of Master of Science in Chemical and Materials Engineering

School of Engineering and Digital Sciences
Department of Chemical and Materials Engineering

Awal Adava Abdulsalam (202243983)

Supervisor: Professor Stavros. G. Poulopoulos
Co-supervisor: Professor Boris Golman

2025

DECLARATION

I hereby, declare that this manuscript, entitled “Kaolin-Based Adsorbent for Environmental Applications,” is the result of my own work except for quotations and citations which have been duly acknowledged.

I also declare that, to the best of my knowledge and belief, it has not been previously or concurrently submitted, in whole or in part, for any other degree or diploma at Nazarbayev University or any other national or international institution.

Name: Awal Adava Abdulsalam

Date: 8th April 2025

ABSTRACT

Mercury contamination remains a critical global concern owing to its persistence, toxicity, and tendency to bioaccumulate within the ecosystem. Conventional methods for mercury remediation, including ion exchange and chemical precipitation, are often hindered by high cost, complexity, sludge generation, or limited regeneration potential. Adsorption has received great interest because of its simplicity, scalability, efficiency, and ability to minimize the generation of harmful sludge. However, most adsorbents used in adsorption processes are in their powdered form, thereby posing challenges in terms of handling and regeneration.

In this thesis, a novel kaolin-based pellet adsorbent was developed and systematically investigated to address these shortcomings. Natural kaolin was initially calcined and subjected to sequential acid–base treatments to enhance its pore structure and expose additional active sites. The surface of the treated kaolin was then functionalized with 3-mercaptopropyltrimethoxysilane (3-MPTS) to introduce thiol groups, thereby strengthening mercury-binding capabilities. The functionalized kaolin was subsequently shaped into pellets via extrusion in the presence of a polyvinyl alcohol (PVA) binder.

Comprehensive physicochemical characterizations using X-ray fluorescence, X-ray diffraction, scanning electron microscopy, Fourier transform infrared spectroscopy, energy-dispersive spectroscopy, Brunauer–Emmett–Teller surface analysis, and zeta potential measurements confirmed that acid–base modification and thiol grafting markedly improved the surface properties of kaolin and its affinity for mercury ions. Batch adsorption experiments revealed that mercury uptake was strongly dependent on contact time, solution pH, adsorbent dosage, and pellet size. Equilibrium was reached at 48 h, with a removal efficiency of 64.2%–79.1% across the studied temperature range (293–313 K). Adsorption kinetics fit the pseudo-second-order model ($R^2 > 0.98$), signifying chemisorption as the dominant mechanism. Thermodynamic parameters ($\Delta H = 18.8$ kJ/mol; $\Delta S = 55.7$ J/molK) indicated an endothermic and spontaneous process, with negative ΔG values over all temperatures tested. Desorption experiments using ethylenediaminetetraacetic acid disodium salt dihydrate and potassium iodide confirmed that mercury was strongly bound to the thiol-functionalized surface, reflecting robust surface complexation or covalent bonding.

These findings open promising avenues for industrial applications, where reliable performance, mechanical stability, and minimal generation of secondary waste streams are critical. Furthermore, the adsorption insight gained herein can guide the design of advanced adsorbents from natural materials for broader heavy metal remediation.

ACKNOWLEDGEMENT

I would like to express my deepest gratitude to my supervisor, Professor Stavros. G. Poulopoulos, for his invaluable guidance, support, and encouragement throughout this research. His insightful feedback and expertise have been instrumental in helping me navigate the challenges of this thesis. I would also like to extend my heartfelt appreciation to my co-supervisor, Professor Boris Golman, for his continued advice and assistance. His dedication and insights were crucial to the success of this work.

I wish to acknowledge the Department of Chemical and Materials Engineering for providing an excellent academic environment that fostered my growth as a researcher. Special thanks go to the Core Facilities team at Nazarbayev University, who assisted me with equipment training and sample characterization. Their expertise and dedication greatly facilitated my research.

I am sincerely grateful to the Abay Kunabayev Scholarship, provided by the Kazakhstan government through Nazarbayev University, for the financial support that enabled me to pursue this Master's program.

Finally, I would like to thank my family, friends, and research colleagues for their unwavering support and encouragement throughout my studies. Their belief in me has been a constant source of motivation, and I could not have completed this journey without them.

TABLE OF CONTENTS

LIST OF TABLES

LIST OF FIGURES

CHAPTER ONE: INTRODUCTION

1.1. Background

Mercury contamination in water bodies is a global issue because mercury is not only highly toxic but also remains in the environment for long periods. Unlike other pollutants, mercury does not degrade over time and instead accumulates in living organisms, threatening human and ecosystem health via the food chain (Ahmad et al., 2022). Industrial activities exacerbate this issue. For instance, in Kazakhstan, elevated mercury levels have been recorded in Lake Balkyldak (∼11 km north of Pavlodar city) and the Nura River, largely attributable to industrial effluents (Guney et al., 2020). Similar challenges plague many regions worldwide, where mercury-contaminated wastewater arises from chlor-alkali plants, fossil fuel combustion, and mining operations (Teng and Altaf, 2022; Kumar et al., 2020).

As mercury continues to contaminate waterbodies, human exposure through the consumption of contaminated fish and seafood is a continuous public concern. Accumulation of methylmercury in various species of fish renders them unsafe for consumption (Kerdoun et al., 2024; Goyanna et al., 2022). Exposure to such can lead to severe complications such as neurodevelopmental disorders, internal organ damage, and chronic reproductive, cardiovascular, and neurologic effects (Balali-Mood et al., 2021; Dack et al., 2022; Bjørklund et al., 2019; Genchi et al., 2017). In response, global organizations like the World Health Organization (WHO) have established strict mercury limits for drinking water, which has prompted regulatory measures in most countries (Vareda et al., 2019). However, enforcing these standards remains challenging, particularly in the absence of cost-effective and efficient remediation strategies.

Researchers have developed a range of methods to remove mercury from water systems, including techniques like ion exchange (Cardoso et al., 2021), membrane filtration (Islam et al., 2020), and adsorption (Al-Ghouti et al., 2019). Of these methods, adsorption has received great interest because it is simple, scalable, and efficient (Qasem et al., 2021; Hua et al., 2020). Additionally, adsorption minimizes the generation of harmful sludge, one major shortcoming with technologies such as chemical precipitation or coagulation and flocculation (Benalia et al., 2022; Zhao et al., 2021). On the one hand, several advanced adsorbents such as metal–organic frameworks (MOFs)

(Fu et al., 2022), graphene-based materials (Huang et al., 2019), and carbon nanotubes (Fayazi, 2020) have been employed to remove mercury from aqueous solution. These advanced adsorbents, despite their promising features, are often costly, require complex synthesis steps, and may pose scalability challenges for large-volume wastewater treatment. Additionally, other concerns include regeneration difficulties and the risk of secondary contamination if nanoparticles or fine particulates from these adsorbents get into the environment (Nayak, 2021; Arayachukiat et al., 2022). On the other hand, conventional adsorbents such as activated carbon (Rao et al., 2009), zeolites (Chojnacki et al., 2004), and biochar (Park et al., 2019) have all proven capable of mercury removal. However, issues concerning cost and regeneration restrict their large-scale application. As a result, there has been growing research toward more abundant, affordable adsorbents, such as natural clays, with kaolin emerging as a promising candidate.

Kaolin, primarily composed of kaolinite, is widely available, inexpensive, and environmentally benign (Alali, 2020). Its layered framework, consisting of tetrahedral and octahedral sheets, can be chemically or thermally modified to enhance its capacity for mercury uptake (Altunkaynak et al., 2023). However, raw kaolin alone often exhibits limited adsorption potential, prompting investigations into calcination, acid–base treatments, and chemical functionalization (Lenarda et al., 2007; Barakan and Aghazadeh, 2021). These modifications typically increase surface area, porosity, and active sites, thereby enhancing mercury adsorption (Belver et al., 2002; David et al., 2020). Functional groups like thiols further solidify mercury binding to form strong chemical bonds (Huang et al., 2017; Pei et al., 2022). Although many of these modifications have proved successful in powdered kaolin, deploying fine powders at industrial scales can lead to issues such as column clogging and difficulties in adsorbent recovery.

To address this, pelletizing kaolin is a good strategy to improve mechanical strength, ease of handling, and operational efficiency, particularly in industrial applications. Pellets improve flow dynamics by promoting uniform distribution of the solution, reducing pressure drop across the bed, and enhancing mixing efficiency, which collectively increase contact between mercury ions and active sites, thereby improving overall adsorption capacity. While the pelleting technique has been investigated for other materials, limited research exists on kaolin pellets specifically for mercury removal (Jurgelane et al., 2013; Bazargan et al., 2016; Tang et al., 2022). This gap

highlights the need to investigate kaolin-based pellets as a practical and economical alternative adsorbent to conventional powder-based adsorbents.

1.2. Problem Statement

Mercury contamination in aquatic environments remains a global challenge, posing a substantial threat to both public health and environmental sustainability. Mercury's well-documented toxicity and persistence result in its accumulation and long-term presence within ecosystems. In Kazakhstan, for example, despite rigorous environmental regulations, elevated mercury concentrations have been identified in Lake Balkyldak and the Nura River, predominantly due to regional industrial activities. While several treatment methods such as ion exchange, membrane filtration, and chemical precipitation have been explored to remove mercury, issues like high cost, complex operation, sludge generation, and limitations in adsorbent regeneration persist. Kaolin, an abundant and environmentally benign clay mineral, has emerged as a promising low-cost adsorbent. However, its powdered form often suffers from limited adsorption capacity and operational handling problems in industrial applications. Pelletizing kaolin holds the potential for enhancing mechanical strength, ease of handling, and process efficiency, but limited research exists on its performance in mercury removal, particularly concerning the role of pellet size, surface modification, and operating parameters. This gap underscores the need to develop, optimize, and systematically study kaolin-based pellet adsorbents for practical, large-scale mercury remediation.

In this thesis, kaolin-based pellet adsorbents are developed and optimized for mercury adsorption from aqueous solution. The study focused on determining how pellet size (using diameter) and surface treatments influence mercury removal. In addition, optimal pH, adsorbent dosage, temperature, and initial mercury concentrations are identified for maximum mercury uptake. Equilibrium studies under different temperature conditions are investigated to determine isothermal behaviors, while kinetic and thermodynamic studies are conducted to shed light on the adsorption mechanisms. By systematically evaluating these conditions and thoroughly characterizing the adsorbents, this research will pave the way for scaling up kaolin pellet applications in industrial wastewater treatment.

1.3. Research Objectives

The main purpose of this thesis is to address the issue of mercury in wastewater. This will be achieved by developing a pellet-based adsorbent from natural kaolin through extrusion. The objectives of this thesis are as follows:

- To investigate how pellet sizes and different treatment methods affect mercury adsorption.
- To determine the optimal pH, adsorbent dosage, temperature, and initial mercury concentration for maximizing mercury removal.
- To study kinetics, isotherm at different temperatures, and thermodynamics of the adsorption process.

1.4. Research Questions

This study is designed to answer the following research questions:

- How do pellet sizes and surface treatment affect the physical, chemical, and structural properties of kaolin pellets?
- What are the optimum operating conditions (pH, adsorbent dosage, contact time, temperature, and initial concentration) for achieving maximum mercury removal using kaolin-based pellet adsorbents?
- How do the kinetic and thermodynamic parameters inform the mechanism of mercury adsorption onto kaolin-based pellets?
- Can the adsorption process be readily reversed, and what is the strength of the adsorption mechanism?

1.5. Organization of the Thesis

This thesis is structured into five chapters. Chapter 1 presents the introduction to the research work, including an overview of the study, problem statement, research objectives, and research questions. Chapter 2 provides a critical review of the literature, with a major focus being laid on mercury pollution and its harmful health impacts, as well as established processes for mercury removal from water systems. Chapter 2 also presents an overview of kaolin as a low-cost adsorbent material, as well as different modifications to enhance kaolin’s performance. Chapter 3 describes research methodology for the modification of kaolin, production of kaolin pellets, as well as adsorption experimental processes. Chapter 4 describes experimental results with an analysis of

results and their correlations with pertinent studies. Chapter 5 summarizes the overall findings, drawing conclusions based on the research conducted and suggesting areas for further investigation.

CHAPTER TWO: LITERATURE REVIEW

2.1. Overview

Water pollution from heavy metals presents a great challenge to environmental protection due to their toxic effects on human health. In this section, an extensive literature review is presented, discussing heavy metals pollution, particularly mercury, and its health effects on humans. Additionally, it discusses different treatment methods, focusing on adsorption and kaolin pelletization.

2.2. Heavy Metals

In the modern era, environmental pollution is an ever-increasing concern due to its adverse effects on public health. One source of these health hazards is toxic metals that are industrially released into water bodies. Heavy metals are naturally occurring elements that have a high atomic weight and density, existing as either essential or non-essential. Essential heavy metals are necessary for vital biological activities in humans and aid in the growth of plants. However, non-essential heavy metals are toxic and can have an effect on human health when they get into the environment (Edelstein and Ben-Hur, 2018). Essential heavy metals become harmful when their concentration exceeds the regulatory threshold limit. According to the World Health Organization (WHO), the heavy metals of primary concern to humans include lead, zinc, copper, nickel, chromium, mercury, cadmium, and arsenic.

Several studies have been conducted to determine the presence of heavy metals in the environment. For instance, Ahamad et al. (2024) conducted a case study on River Ravi, Pakistan, to determine the impact of heavy metals on human and aquatic life. They focused on pollution levels, risk, and mitigation measures and found that cadmium showed varying pollution levels, ranging from moderate to significant. Additionally, noncarcinogenic and carcinogenic risks exceeded safe limits for cadmium, arsenic, copper, nickel, and chromium, especially in children. Ogarekpe et al. (2023) assessed groundwater quality and human health risk to heavy metals in Calabar, Nigeria. Heavy metals such as chromium and zinc were found in groundwater samples, posing a significant noncarcinogenic health risk to adults and children. Khan et al. (2021) took a close look at how contaminated the Gomti River is with heavy metals and assessed the potential health risks posed

to people who rely on its water. They found that heavy metal contamination in this river poses high health risks to millions due to sewage and industrial effluents exceeding permissible limits, especially impacting children, and recommended the need to act immediately to bring down the high heavy metal levels at every sampling station. Exposure to elevated levels of heavy metals may produce different toxic responses in the human body in the short term (acute toxicity) or when exposed over a long period of time (chronic toxicity). These exposures may lead to different types of health effects such as cardiovascular, central nervous system, liver, kidney, bone, and skin disorders or cancer. Table 2.1 presents the maximum heavy metal concentrations permitted in drinking water, as specified by the World Health Organization, the United States, the European Union, Canada, and China.

Table 2.1. Maximum concentration level (MCL) of heavy metals in drinking water (Vareda et al., 2019)

Heavy Metal	MCL in drinking water/μgL^{-1}				
	WHO	EU	USA	Canada	China
Arsenic	10	10	10	10	10
Cadmium	3	5	5	5	5
Chromium	50	50	100	50	50
Copper	2000	2000	1300	-	1000
Lead	10	10	15	10	10
Mercury	6	1	2	1	-
Nickel	7	20	-	-	20
Zinc	-	-	-	-	1000

2.3. Mercury Pollution

Mercury is particularly dangerous due to its ability to accumulate in fish and seafood, leading to potential risks for human brain development (Ahmad et al., 2022). Natural sources of mercury include volcanic eruption and rock weathering. However, significant amounts of mercury are also released through human activities such as fossil fuel combustion, solid waste incineration, chlor-alkali production, and the extraction of gold and silver. For example, in Kazakhstan, substantial

mercury contamination originates from industrial sources such as the carbide-acetaldehyde plant in Temirtau and the chlor-alkali plant in Pavlodar. These facilities discharged large quantities of mercury into nearby water bodies, including Lake Balkyldak and the Nura River (Guney et al., 2020). Mercury in the environment exists in three forms: metallic, inorganic, and organic (Teng and Altaf, 2022). Upon release, mercury deposits enter the atmosphere, dissolve in water, and are converted into methyl mercury by bacteria in water or sediment. These organic forms of mercury are highly toxic and bioaccumulate in the food chain, making them especially hazardous (Kumar et al., 2022). Figure 2.1 shows a pathway of mercury exposure to humans.

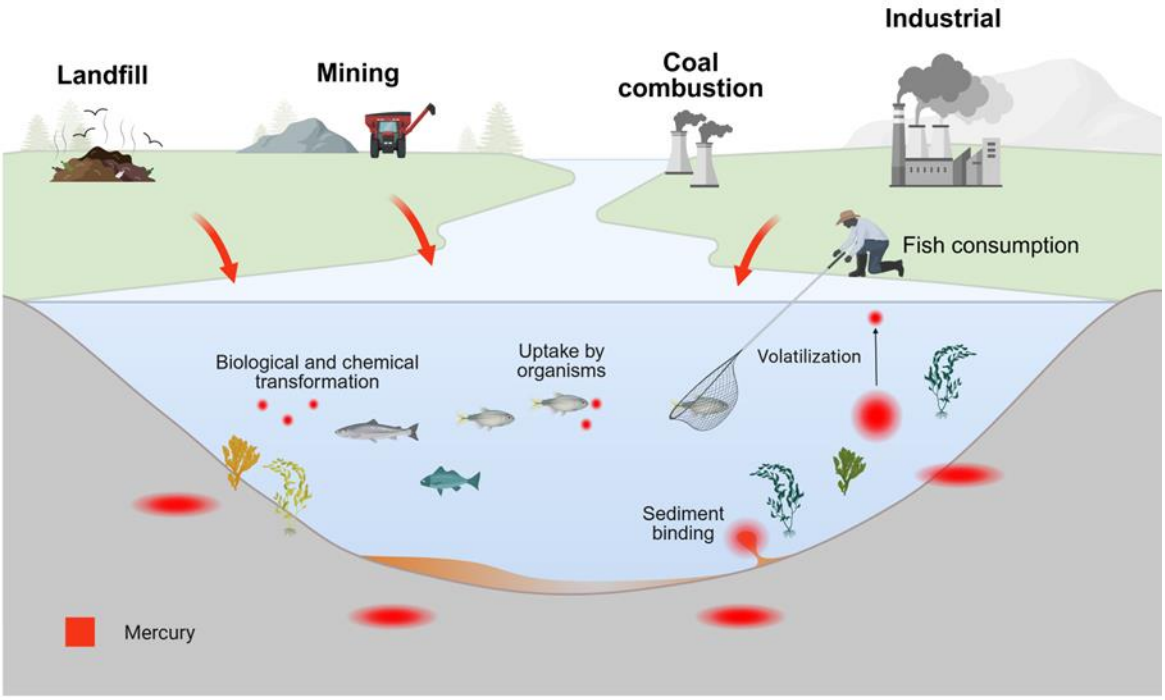

Figure 2.1. Pathway of mercury into the human body

High concentrations of methylmercury have been reported in fish, and this has raised serious concerns regarding the toxicity of mercury to consumers (Barone et al., 2021). A comprehensive survey conducted in Algeria revealed the mean concentration of mercury to be 0.19 mg/kg in four fish species, with the highest concentration recorded in *Sparus aurata* at 0.27 mg/kg (Kerdoun et al., 2024). In the subarctic lakes in Canada, the concentration of mercury in fish was found to be directly related to catchment-to-lake ratios, with the implication that the proportionately larger

catchment areas in small lakes held greater amounts of mercury burden (Aqdam et al., 2024). Moreover, studies have shown that top predator species such as sharks and tunas commonly record mercury content beyond the 1 ppm safety threshold (Goyanna et al., 2022). Thus, the consumption of such predator fish can be dangerous to one's health, and this necessitates raising awareness about the occurrence of mercury in seafood.

2.3.1. Health Impact of Mercury

Human exposure to mercury primarily occurs through the consumption of fish with elevated methylmercury levels. Such exposure poses significant risks, including damage to multiple organ systems and, in pregnant women, adverse effects on the developing brain and nervous system of the fetus. In more severe cases, studies have linked high-level exposure in children to significant neurological problems, including intellectual disability, cerebral palsy, deafness, and blindness (Dack et al., 2022). Mercury poisoning, especially in children exposed to even low levels, is known to impair vital physiological systems and disrupt cognitive functions, including reasoning and memory (Balali-Mood et al., 2021).

Extensive research has elucidated the toxicological impact of mercury on human health. Kumar et al. (2022) conducted a comprehensive review of occupational and environmental mercury exposure and its effects on reproductive health, demonstrating that such exposure can exert toxic effects on the reproductive system, thereby disrupting fertility, altering reproductive hormone levels, and influencing pregnancy outcomes. Similarly, Bjørklund et al. (2019) highlighted the relation between mercury exposure and increased risks of congenital malformations in newborns, spontaneous abortion, and reduced fertility. Their findings further indicate that mercury can contribute to irregular menstrual cycles, testicular degeneration, and impaired reproductive capacity. In another study, Genchi et al. (2017) investigated the cardiovascular consequences of mercury poisoning, concluding that chronic exposure compromises cardiac health and function while also inducing reproductive and developmental toxicity alongside neurotoxicity, nephrotoxicity, immunotoxicity, and carcinogenicity. Collectively, these studies underscore the critical need for heightened awareness and robust preventive measures to limit environmental mercury exposure. The evidence suggests that the deleterious health effects of mercury are severe

and, in some cases, potentially fatal, necessitating immediate action to mitigate its presence and impact.

2.3.2. Removal of Mercury from Water Systems

The bioaccumulation potential and resistance to degradation by mercury pose dangers to the food chain and aquatic life globally (Al-Sulaiti et al., 2022). Stringent measures to limit its occurrence in wastewater have been established, but compliance is difficult if cost-effective treatment methods are not available. Treatment methods available include adsorption (Al-Ghouti et al., 2019), ion exchange (Cardoso et al., 2021), membrane filtration (Islam et al., 2020), and chemical precipitation (Li et al., 2015). However, each method has some drawbacks: excessive reagent consumption, generation of toxic sludge, or contamination of the treated effluent. Adsorption has emerged as the most promising option owing to its efficiency at a relatively economical cost (Qasem et al., 2021). Table 2.2 highlights the benefits and limitations of these methods.

Table 2.2. Advantages and limitations of different mercury treatment methods

Method	Advantages	Limitations	Source
Ion exchange	High selectivity Fast kinetics	Resins have to be regenerated High cost	(Qasem et al., 2021)
Chemical precipitation	Low energy required Low cost	Generate a high volume of sludge, which requires disposal	(Benalia et al.2022)
Membrane filtration	High efficiency	Membrane fouling High energy consumption	(Xiang et al.2022)
Coagulation–flocculation	Rapid settling of suspended solids Can be combined with other treatment methods	Sludge production, which requires disposal	(Zhao et al.2021)
Adsorption	High efficiency Low cost of adsorbent	Fast saturation of adsorbent material requiring regeneration	(Hua et al., 2020)

2.3.3. Adsorption

Adsorption is a surface phenomenon that involves the accumulation of molecules on the surface of a material. It is primarily used to separate and purify mixed components. This process is either through physical or chemical attachment of the pollutant on a porous adsorbent, decreasing the concentration of the pollutant. Physical adsorption occurs when a pollutant such as mercury is adsorbed onto the surface of materials via van der Waals forces. Factors such as surface area, pore size, and structure play a key role in the effective adsorption of the pollutant. Particles that contain moderate pore volumes and large surface areas take up large amounts of pollutants by way of surface capturing and polarization phenomena. Chemical adsorption, on the other hand, is recognized by the formation of chemical bonding between adsorbent and adsorbate surfaces. For example, functionalized montmorillonite has shown enhanced performance in this context (Pei et al., 2022). Chemical bonding in this mechanism causes the desorption of adsorbed contaminants to be difficult. In the adsorption of Hg^{2+} utilizing thiol-functionalized montmorillonite, for example, chemical interactions are formed between the adsorbate (Hg^{2+}) and the adsorbent functional groups (thiol), therefore rendering reversibility a problem (Pie et al., 2022). The development of a Hg–S bond explains this reversibility and shows the stability of chemosorption.

Recently, researchers in material science have developed several innovative adsorbents for mercury removal, such as MOFs (Fu et al., 2022), graphene-based materials (Huang et al., 2019), and carbon nanotubes (Fayazi, 2020). MOFs, for example, can be designed with customizable pore structures, exceptionally high surface areas, and functional groups tailored for specific pollutants (Nayak, 2021). Graphene and carbon nanotubes also exhibit high surface area and unique electronic properties that allow efficient binding for mercury ions (Yu et al., 2018). However, despite these promising features, these advanced adsorbents can be expensive to produce, often require complex synthesis steps, and may be challenging to scale up for treating large volumes of wastewater. Additional concerns include regeneration difficulties and the risk of secondary contamination if nanoparticles or fine particulates get into the environment (Nayak, 2021; Arayachukiat et al., 2022). In the context of high cost, high complexity, and sustainability concerns of high-end adsorbents, natural materials such as activated carbon (Rao et al., 2009), biochar (Park et al., 2019), zeolites (Chojnacki et al., 2004), and clay minerals (Wang et al., 2020) have been viewed as low-cost and environmentally friendly alternatives for mercury removal. The

performance of these adsorbents is influenced by several factors, including temperature, pH, and the initial mercury concentration (Akhtar et al., 2016). The process through which these adsorbents adsorb the target mercury can be from a variety of interactions. These interactions include electrostatic forces, π–π interactions, hydrogen bonding, ion exchange mechanisms, and surface complexation. The process of adsorption can be further enhanced by controlling variables like temperature, pH, and the ratio of the material to be adsorbed onto the adsorbent (Mustapha et al., 2022).

Several studies have been conducted on how these adsorbents can be used to remove mercury from water. In a previous study, researchers discovered that conventional activated carbon is not very effective at removing mercury, largely due to its structural properties (Liu et al., 2023). However, zeolite-templated carbon, through physisorption and chemisorption at varying temperatures, has been found to be efficient for the removal of mercury from aqueous solution due to its ordered porosity (Liu et al., 2023). Biochar modified with HNO_3 and NH_4Br has demonstrated effectiveness in removing mercury, where approximately 100% removal efficiency was achieved at optimal temperatures due to the formation of reactive functional groups (Zeng et al., 2023). Natural zeolites modified with silver have also proven effective in removing mercury from aqueous solution, where they outperformed commercial adsorbents in certain conditions (Inglezakis et al., 2023). Here, the interaction between ion exchange and surface reactions plays a crucial role in their effectiveness. Clay minerals, such as bentonite combined with biochar, have been shown to exhibit high mercury removal, up to 98%, under optimal conditions (Arif et al., 2021). The effectiveness of these adsorbents is greatly influenced by factors like pH levels and the presence of competing ions, which have a significant impact on their overall performance. At lower pH conditions ($pH < 4$), protonation of adsorption sites will decrease electrostatic interactions, and hence, overall mercury absorption will be lowered (Pei et al., 2022). By contrast, at high pH conditions ($pH > 8$), mercury tends to precipitate or form hydrolyzed complexes (e.g., $Hg(OH)_2$), which are less prone to adsorb onto negatively charged surfaces (Huang et al., 2020; Huang et al., 2023). Consequently, there is usually an optimal pH range, typically between 5 and 7, at which the functional groups on the adsorbent surfaces are deprotonated, thereby making them available for effective electrostatic and/or chemical interactions with Hg^{2+} ions (Huang et al., 2017; Pei et al., 2022). Moreover, the presence of competing ions such as Ca^{2+}, Cl^-, and SO_4^{2-} can reduce the

adsorption of mercury by occupying the same active sites (Huang et al., 2019). For instance, some anions can form soluble complexes with mercury, preventing it from interacting with the active sites of the adsorbent, while other cations may shield or outcompete mercury ions for binding locations (Xiao & Thomas, 2004). Consequently, high concentrations of competing ions in the water matrix often necessitate further optimization of adsorption parameters or additional pre-treatment steps. While these conventional adsorbents have shown effective removal of mercury, the comparatively high price of some of them, such as activated carbon, necessitates a search for cheaper and available alternatives. Clay minerals have shown potential due to their cost effectiveness and availability, making them excellent candidates for industrial-scale mercury removal.

2.4. Kaolin

Kaolin is one of the most abundant natural clay minerals, and it majorly consists of the mineral kaolinite, a hydrous silicate of aluminates. It is a two-layered structure consisting of a tetrahedral sheet (silicon and oxygen) and an octahedral sheet (aluminum, oxygen, and hydroxyl groups), as shown in Figure 2.2 (Alali, 2020). Kaolin has natural properties such as low cost, zero toxicity, minimal health effects, low flammability, and good solubility. These properties are mainly due to kaolin being a silicate that contains minerals like kaolinite. Kaolin offers several physical advantages as an adsorbent, such as its fine particle size and surface area, which, compared to other aluminosilicates, provides more exposed sites for the adsorption of gases or liquids. In addition, the low cost and natural abundance of kaolin make it a feasible choice for large-scale environmental applications. According to Sigma Aldrich, the price of 100 g of zeolite goes for 137 euros, while 2.5 kg of kaolin goes for 101 euros. Additionally, in Kazakhstan, kaolin costs 310 tenge per kilogram, while activated carbon costs 1498 tenge per kilogram, and the Alekseevskoye deposit in the Akmola region is expected to produce 90,000 tonnes of enriched kaolin annually. This indicates how significantly cheap kaolin is compared to other adsorbents such as zeolite and activated carbon.

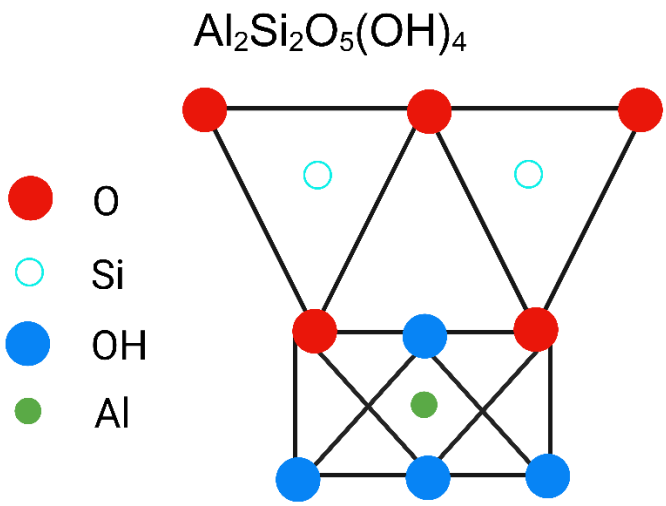

Figure 2.2. Structure of kaolin

2.4.1. Kaolin as Adsorbent for Mercury Adsorption

Kaolin, which is rich in Si–O and Al–O groups, is thought to have an affinity for mercury, providing a significant advantage in mercury adsorption. A previous study indicated that natural kaolin exhibits an adsorption capacity at a maximum of10.964 mg/g for mercury removal under optimal conditions of pH 6.81 and 90-min contact time (Altunkaynak et al., 2023). However, kaolin has a low adsorption capacity, highlighting the need to investigate the limitations of kaolinite as a potential adsorbent for mercury and explore how it can be enhanced. The physicochemical properties of kaolin can be enhanced through thermal treatment, acid-base treatment, impregnation, or functionalization with organic or inorganic agents (Barakan and Aghazadeh, 2021). These processes can enhance its surface area, porosity, and chemical active sites, making kaolin suitable for specific mercury removal and increasing its adsorption capacity.

2.4.2. Treatment of Kaolin

Thermal activation

Raw kaolin has been found through Bragg reflection to contain impurities such as aluminum in its layered structure, extending beyond its basal region. However, these impurities can be removed upon thermal activation (calcination), indicating that mercury can be immobilized within activated kaolin (Ding et al., 2021). Generally, calcination temperatures of kaolin range between 600°C and 900°C, which is mostly dependent on the origin of the kaolin. The dehydroxylation process during calcination usually occurs between this temperature range, converting kaolin into metakaolin.

However, temperature above this range converts metakaolin into a defect, forming a crystalline phase. Note that increasing the temperature during kaolin calcination results in decreased surface area and increased pore volume (Wang et al., 2011). According to Anagho et al. (2013), using kaolin and metakaolin to remove mercury from water can achieve removal rates of 45.18% and 71.65%, respectively. Thermal modification of kaolin affects its surface area but does not markedly impact its mercury adsorption from water.

Acid–base treatment

Acid and base treatments have been mostly used to enhance the surface area of kaolin. Belver et al. (2002) enhanced the surface area of kaolin to up to 219 m^2/g by treating it with acid and base. They performed acid activation with 6 M HCl at room temperature, and the treatment duration ranged from 6 to 24 h. The acid treatment resulted in the dissolution of the octahedral Al^{3+} cations, thus forming an amorphous silica phase. They also treated the kaolin with 1 and 5 M KOH solution at room temperature. This dissolved the kaolin and formed well-crystallized zeolite. David et al. (2020) modified kaolin using both thermal and hydrothermal alkaline treatments to enhance its ability to remove lead. They used three different preparations: 2.5 M of NaOH for 7 h, 1.5 M of NaOH for 8 h, and 1.5 M of NaOH for 11 h. Their result showed a significant increase in the surface area of kaolin, which was elevated from 19.170 m^2/g to 247.889, 208.745, and 221.608 m^2/g, respectively. Similarly, Lenarda et al. (2007) highlighted that kaolin thermally activated and then acid-modified is effective in removing mercury from aqueous solution. Note that acid activation alone is inefficient in removing mercury due to the inactive nature of kaolin in its regular structure. This challenge is mitigated when calcination is conducted before acid treatment. Metakaolin is more reactive compared to kaolin, making treatments such as acid treatments more effective with metakaolin (Lenarda et al., 2007).

Surface modification

While it is important for heavy metals such as mercury to be adsorbed onto kaolin, surface adsorption alone may allow the adsorbed mercury to re-enter the environment. Therefore, it is beneficial for kaolin to have an internal structure that can trap the molecule. Mercury molecules should be firmly attached to the surface groups and interior of kaolin and should not be displaced by competing molecules. Grafting agents such as 3-mercaptopropyltrimethoxysilane (3-MPTS) and other silane coupling agents are frequently employed to enhance the adsorption of mercury

through thiol groups. Pei et al. (2022) prepared thiol-functionalized montmorillonite for the immobilization of mercury in contaminated media, reporting intercalation and grafting methods. Similarly, Pei et al. (2022) synthesized thiol-functionalized montmorillonite by the use of mechanochemical grafting for the adsorption of methylmercury and mercury. They obtained an adsorption capacity at a maximum of 104.79 and 39.27 mg/g for mercury and methylmercury, respectively. Wang et al. (2019) employed montmorillonite that was functionalized with thiol groups and modified with an organic surfactant to stabilize soils contaminated with varying mercury concentrations. They obtained a stabilization efficiency of greater than 90% for the soils after grafting montmorillonite with the thiol group. This indicates that the stabilization capacity of the montmorillonite-modified organic surfactant was highly influenced by the thiol group, which made it efficient in removing mercury from contaminated soils. Studies have also shown that the adsorption functionality for mercury is enhanced by treating raw kaolin with geopolymers, resulting in excellent adsorption performance from the chemically altered kaolin. Santos et al., 2022 showed that metakaolin-based geopolymers are effective for mercury removal, where they acheved a removal efficiency of 65.1% and an adsorption capacity of 38.1 mg/g. Table 2.3 summarize studies on the use of kaolin for mercury adsorption. Note that kaolin is typically used in its powdered form in most studies. Unfortunately, this form is faced with major limitations in terms of handling and recovery. Despite this challenge, there are limited or no studies on pellet kaolin adsorbents. This is because when not used as an adsorbent or catalyst, kaolin is mostly used as a binder for other chemicals.

Table 2.3. Summary of studies on the use of kaolin for mercury adsorption

Reference	Powder size	Treatment	Mercury concentration (mg/L)	Equilibrium time	Adsorption capacity (mg/g)	Removal (%)
Altunkaynak et al. 2024	<100 µm	No treatment	90	300 min	10.1–10.9	-
Anagho et al. 2013	≤2 µm	Thermal activation at 700°C	350–500	40 min	-	71.65
Yilmaz et al. 2017	≤125 µm	Modified with 3-MPTS	30.83	150 min	30.10	98.01
Lin et al. 2020	-	Polypyrrole functionalized Fe_3O_4	50	480 min	317.7	-
Santos et al. 2022	150 µm	Alkaline activation using Sodium hydroxide and sodium silicate solutions for geopolymerization	50	5 h	38	65.1
Rao et al. 2023	75 µm	Thermal activation at 750°C and alkaline activation using sodium silicate solutions for geopolymerization	100	300 min	-	65
Xu et al. 2022	-	L-cysteine and Polypyrrole functionalized Fe_3O_4	40–60	8 h	482.71	-

2.5. Kaolin Pellets

Pelleting adsorbents, including kaolin, enhance mechanical strength and handling. Common pelletizing techniques include extrusion, compaction, and compression. Among these techniques, extrusion is the most popular. In this process, raw kaolin powder is mixed with water and then extruded. After obtaining a solid extrudate, it is dried to solidify the sample. The primary advantage of extrusion is the homogeneity of the raw powders, which pass through the extrusion die under a certain extrusion force. As a result, extrusion can produce shape-deformed absorbents with specific porosity. Therefore, the choice of extrusion die is crucial.

Pelletizing kaolin offers several benefits over using powder forms, particularly in fixed-bed columns. Pellets improve flow dynamics by promoting uniform distribution of solution, reducing pressure drop across the bed, and enhancing mixing efficiency, which collectively increase contact between mercury ions and active sites, thereby improving overall adsorption capacity. This results in improved operational performance, making pellets more practical and efficient for pollutant removal. The use of pelletized adsorbents also prevents column plugging and improves resistance to stress in liquid-solid systems, contributing to better performance in industrial settings. In addition, binders are essential in increasing the mechanical strength during the pelletization process. There is also scarce research focusing directly on the use of kaolin as pellets for the adsorption of mercury. However, research has been conducted on other adsorbents, including zeolite and activated carbon, heavy metal adsorption. Chow et al. (2023) conducted adsorption studies using zeolite–water hyacinth ash–clay pellets for zinc, copper, and lead adsorption from aqueous solutions. This research involved different pellet formulations and pellet sizes, as well as pretreatment processes and their impacts on the pellets. According to their optimization analysis, smaller pellet sizes, as well as those pretreated with the solution of calcium hydroxide, had better removal efficiency, with percentages of 84, 86, and 91 for zinc, copper, and lead, respectively. Li et al. (2017) synthesized ceramic pellets for the adsorption of phosphorus. Their synthesized pellet, which had a diameter and length of 4 mm and 1 cm, respectively, had an adsorption capacity at a maximum of 1.98 mg/g. Bazargan et al. (2016) prepared pellets with an aluminosilicate-based adsorbent and tested their mechanical strength through varying ratios of a binder consisting of calcium carbonate. They revealed that binder content as low as 2.5 wt% in combination with 30% moisture showed resistance to compaction pressures of up to 80 MPa. Water-resistant pellets were

also prepared in another study conducted by Tang et al. (2022) with sludge-activated carbon powder blended using phosphoric acid-impregnated sawdust as an economical binder. They revealed that pellets retained their cylindrical shape when used in the adsorption of malachite green dye for 3 h, having an adsorption capacity of 395 mg/g. These improvements, illustrated by zeolite–water hyacinth ash–clay pellets, ceramic pellets, and activated carbon–clay composites, underscore the potential of pelletized adsorbents for pollutant removal.

2.6. Research Gap and Novelty of the Thesis

Despite the promising results of kaolin-based adsorbents in mercury remediation, research has largely focused on kaolin in its powdered form. Most studies have emphasized thermal or chemical modifications to enhance adsorption properties of kaolin, with limited or no attention to pelletized kaolin. This poses handling and operational challenges such as column clogging and difficulties in adsorbent recovery at large scales. Although studies on other pelletized adsorbents, like zeolite, activated carbon, and clay-based composites, have demonstrated improved mechanical strength, enhanced flow distribution, and reduced pressure drop, similar investigations on kaolin pellets are scarce. As far as I know, there has been only one study that looked into using kaolin in pellet form for environmental remediation (Jiménez-Bautista et al., 2023). However, the study focused on the photodegradation of pesticides. Furthermore, investigations on these other pellet adsorbents have not been examined for mercury removal nor have they critically investigated factors such as pH, adsorbent dosage, temperature, and initial concentrations of other contaminants. Moreover, regeneration of these other pellet adsorbents has not been thoroughly studied, a crucial factor for sustainable industrial applications.

This thesis seeks to fill these gaps by developing and optimizing kaolin-based pellet adsorbents for mercury removal. It introduces a systematic approach to evaluating the effects of pellet size, surface treatment, and operational parameters (pH, dosage, temperature, and initial mercury concentration) on mercury adsorption. Furthermore, it investigates desorption behavior, isotherms at different temperatures, and kinetic as well as thermodynamic parameters. The novelty lies in providing an integrated investigation, from pellet production and characterization to adsorption performance and mechanism, offering a practical and scalable solution to mercury pollution.

CHAPTER THREE: MATERIALS AND METHODS

3.1. Overview

In this chapter, the treatment, characterization, pellet production, and evaluation of modified kaolin pellets for Hg^{2+} adsorption are presented. The methodology flowchart is displayed in Figure 3.1.

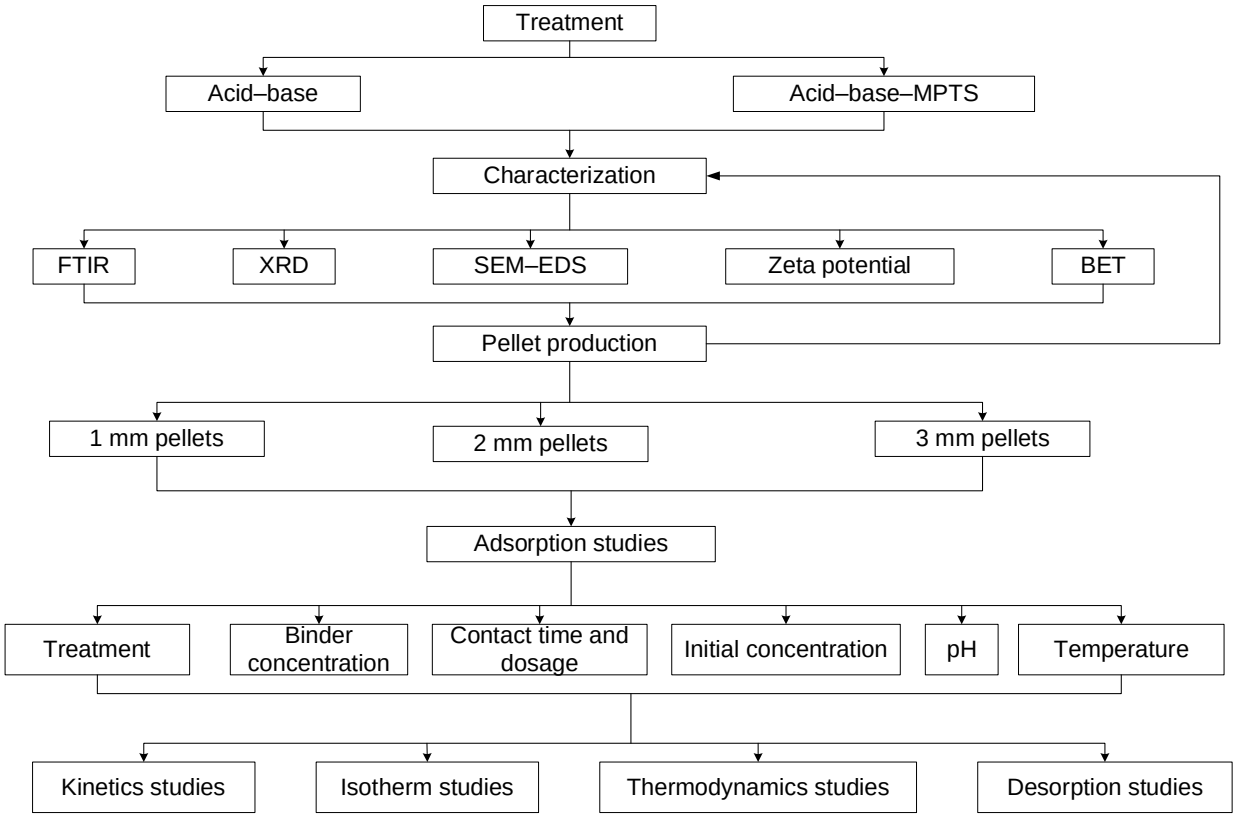

Figure 3.1. Methodology flowchart

3.2. Materials and Chemicals

Raw kaolin (RK) powder was obtained from Supelco (Merck KGaA, Darmstadt, Germany). 3-MPTS (95%), hydrogen chloride (HCl; 37%), sodium hydroxide (NaOH; >97%), polyvinyl alcohol (PVA; 87%–89%), ethanol (96%), ethylenediaminetetraacetic acid disodium salt dihydrate (EDTA $2Na{\cdot}2H_2O$; ≥99%), potassium iodide (KI; 99%), and mercury (II) chloride (≥99.5%), were all purchased from Sigma-Aldrich LTD. All chemicals were of analytical grade or higher and were used as received without additional purification or modification. Deionized water was used throughout the study.

3.3. Chemical Modification of Kaolin

Chemical modification of kaolin was obtained by calcining 30 g of RK. This sample was heated at a rate of 10°C/min until the temperature reached 600°C, and then maintained at that temperature for 5 h. The resulting material was labeled as calcined kaolin (CK). Acid and base treatments were conducted according to the procedure outlined in Belver et al. (2002). CK was treated with 2.5 M of HCl with a CK to acid ratio of 1:10 w/v at 80°C for 7 h to remove impurities such as Al^{3+}. The acid-treated CK was thoroughly rinsed with deionized water until the pH of the wash water reached a neutral value (~7). It was then oven-dried at 90°C for 12 h. The acid-treated CK was subsequently subjected to an alkaline treatment using 0.5 M of NaOH, maintaining the same ratio of 1:10 (w/v) at 80°C for 7 h. The sample was again rinsed with deionized water until the pH of the rinse water approached neutrality, then oven-dried for 12 hours to produce the acid–base–treated kaolin (AB). Next, 20 g of AB was functionalized with 3-MPTS, following the procedure outlined by Pei et al. (2022). In this step, AB was combined with 20 mL of 3-MPTS, 160 mL of ethanol, and 10 mL of deionized water. The mixture was stirred continuously for 6 h at room temperature (25°C). Afterward, it was centrifuged at 4000 rpm for 5 min and washed three times with ethanol and deionized water to remove any residual 3-MPTS. The resulting material, labeled ABM, was filtered, dried at 80°C for 12 h, and stored for further use.

3.4. Extrusion of Modified Kaolin into Pellets

Pellets were produced through extrusion using the Caleva Multi Lab equipment shown in Figure 3.2. The equipment consists of three major components: extruder, spheronizer, and kneader. Ten grams of the stored treated kaolin was placed in the kneading chamber, and 10 mL of deionized water was added dropwise. The equipment was set to rotate at 100 rpm for 2 min during both the kneading and extruding processes. This time was sufficient for the homogeneous mixing of the treated kaolin into a uniform premix. The premix was then introduced into the screw extruder, where die plates with different opening sizes (1, 2, and 3 mm) were used to produce the extrudates. The extrudates were then cut into pellet forms using a stationary knife. Subsequently, the pellets were oven-dried at 80°C for 12 h and sieved to obtain a homogenous size. Figure 3.3 shows the produced extrudate and the different pellet sizes (1, 2, and 3 mm). To maintain the pellets' integrity during adsorption, PVA was introduced as a binder. PVA solutions of varying concentrations (0.5%, 1.5%, 2.5%, and 5% w/w) were used in place of deionized water during the kneading

process. Pellets grafted with thiol and produced with PVA were denoted as ABM–PVA. Table 3.1 summarizes the naming convention used for the different stages of kaolin treatment and modification.

Table 3.1. Description and labeling of kaolin-based samples

Sample description	Label
Raw kaolin	RK
Kaolin calcined at 600°C	CK
Calcined kaolin treated with acid and base	AB
AB grafted with 3-mercaptopropyltrimethoxysilane (3-MPTS)	ABM
ABM extruded into pellets using polyvinyl alcohol (PVA) as binder	ABM–PVA

Figure 3.2. Caleva Multi Lab equipment

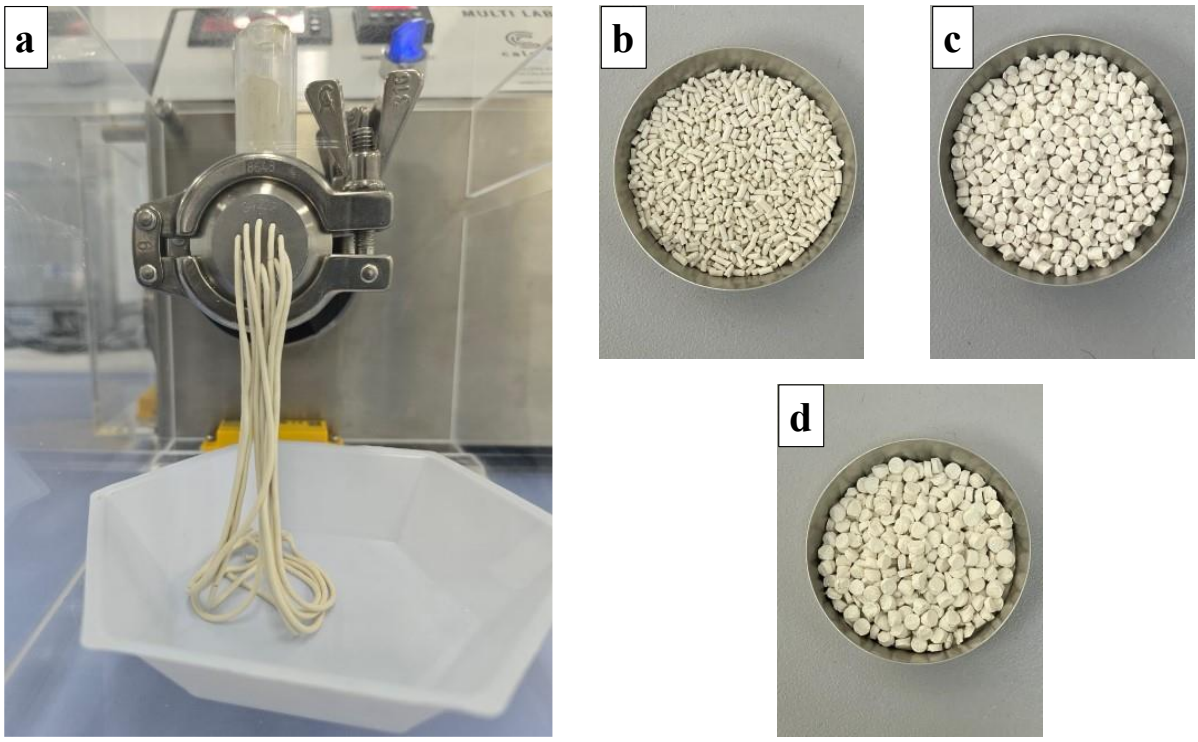

Figure 3.3. a) Produced extrudate, b) 1 mm pellets, c) 2 mm pellets, and d) 3 mm pellets

3.5. Characterization

Characterization of the samples was carried out to assess the effectiveness of the different treatments and their impact on the structure, surface, and functional properties of RK. X-ray diffraction (XRD) analysis was carried out using a Rigaku SmartLab system from Rigaku Corporation (Tokyo, Japan), which features a HyPix-3000 high-energy resolution 2D HPAD detector to provide precise crystallographic information. Diffraction patterns were recorded over a 2θ range of 5° to 60° with a step size of 0.05° at an operating voltage of 40 kV and a current of 40 mA. Chemical composition analysis was carried out using an xrFuse 6 XRF (XRF Scientific, Victoria, Australia). The morphological structure of the samples was examined using scanning electron microscopy (SEM) combined with EDS on a ZEISS Crossbeam 540 (Carl Zeiss AG, Oberkochen, Germany). Nicolet iS10 FTIR spectrometer from Thermo Fisher Scientific (Waltham, MA, USA) was used to analyze the samples, scanning across a wavenumber range of 4000–400 cm^{-1}. This allowed the identification of the different functional groups and bonds present in the material. The specific surface area, pore volume, and pore size of the pellets were determined using Brunauer–Emmett–Teller (BET) surface area analysis on a NovaWin Quantachrome (Quantachrome Instruments, Boynton Beach, FL, USA) at 77.35 K. The specific

surface area was determined using the multipoint BET technique, while the total pore volumes were determined using the amount of nitrogen adsorbed when the relative pressure (P/P_0) reached 0.99. Pore size distributions were then calculated from the adsorption isotherms by applying the density functional theory method. The surface charge of the treated materials was analyzed using a nanoparticle tracking analysis instrument (PMX-230 ZetaView TWIN Laser, Ammersee, Germany). This was determined by measuring their zeta potential as a function of pH.

3.6. Batch Adsorption Experiment

Batch adsorption experiments were performed in 400 mL glass beakers by suspending the pellet adsorbents in a catalyst holder using a clamp, as shown in Figure 3.4. The initial adsorption study was carried out with the AB pellets using three different pellet sizes (1, 2, and 3 mm). In this experiment, 0.5 g of each pellet size was introduced into 200 mL of a 50 mg/L Hg^{2+} solution. The mixture was stirred at a constant speed at room temperature (20°C) till it reached equilibrium. Subsequently, experiments were conducted with the ABM-treated pellets of the same sizes (1, 2, 3 mm) using the same conditions: 0.5 g of pellets, 200 mL, and 50 mg/L of Hg^{2+}. The pellet size with the highest adsorption capacity was selected for further studies. To enhance the mechanical integrity of the pellets, PVA was introduced as a binder at varying concentrations of 0.5%, 1%,1.5%, 2.5%, and 5% (w/w). Pellets were prepared with these binder concentrations and tested for adsorption performance under the same experimental conditions: 0.5 g of adsorbent in 250 mL of a 50 mg/L Hg^{2+} solution. The optimal binder concentration was determined based on both adsorption performance and stability of pellets after the experiment.

Figure 3.4. Batch adsorption setup

Contact time and the effect of adsorbent dosage on Hg^{2+} removal were investigated using the best-performing pellets from the binder concentration study. Dosages of 0.5, 1, 2, and 3 g were tested in 200 mL of 50 mg/L Hg^{2+} solution until equilibrium was achieved. The impact of solution pH on Hg^{2+} adsorption was investigated using the optimal dosage obtained in the dosage study. Initial solution pH values of 3, 5, 7, and 9 were adjusted with 0.1-M NaOH or HCl as required. Finally, the temperature dependence of Hg^{2+} adsorption was investigated at 293 K, 303 K, and 313 K using various initial concentrations (25, 50, 75, 100, and 125 mg/L) and the optimal dosage and pH obtained from previous experiments. All experiments were conducted in duplicate, and average values with standard errors were reported. The concentration of Hg^{2+} in the solution was determined using a mercury analyzer (Lumex RA-915M; Lumex Instruments, St. Petersburg, Russia), and the percentage removal and adsorption capacity (q_e) were calculated using Equations 3.1 and 3.2, respectively.

$$\%Removal = \frac{C_0 - C_e}{C_0} \times 100, \qquad 3.1$$

$$q_e = \frac{C_0 - C_e}{m} \times V \quad . \tag{3.2}$$

Here, C_0 and C_e represent the initial and equilibrium mercury concentrations (mg/L), m is the mass (g) of the adsorbent, and V is the volume (L) of the mercury solution.

For kinetic studies, the adsorption capacity (q_t) of Hg^{2+} adsorbed at time, t, was calculated using Equation 3.3 as follows:

$$q_t = \frac{C_0 - C_t}{m} \times V \quad , \tag{3.3}$$

where C_0 and C_t are the initial concentration (mg/L) of Hg^{2+} and concentration (mg/L) of Hg^{2+} at time, t, respectively, m is the mass (g) of the adsorbent, and V is the volume (L) of the mercury solution.

3.7. Adsorption Kinetics and Isotherms

Pseudo-first order (PFO) and pseudo-second-order (PSO), along with Langmuir and Freundlich isotherms, were used to analyze the adsorption mechanism and performance of Hg^{2+}. PFO and PSO were used to investigate the adsorption mechanism and rate-limiting step, providing insights into whether the adsorption process is governed by chemisorption or diffusion-controlled mechanisms. The nonlinear forms of the PFO and PSO models are presented in Equations 3.4 and 3.5, respectively:

$$q_t = q_m(1 - e^{-K_1 t}) \, , \tag{3.4}$$

$$q_t = \frac{q_m^2 K_2 t}{1 + q_m K_2 t} \, , \tag{3.5}$$

where q_t (mg/g) is the amount of Hg^{2+} adsorbed at time t (h), q_m (mg/g) is the maximum adsorption capacity, K_1 (h^{-1}) is the rate constant for the PFO model, and K_2 (g mg^{-1} h^{-1}) is the rate constant for the PSO model.

To model the adsorption process, the Langmuir isotherm (Langmuir, 1918) was used to describe monolayer adsorption on homogeneous surfaces with uniform binding sites, whereas the Freundlich isotherm (Freundlich, 1907) was used to represent non-ideal (heterogeneous) adsorption, allowing for multilayer coverage. These models are mathematically defined by Equations 3.6 and 3.7, respectively:

$$q_e = \frac{q_m K_L C_e}{1 + K_L C_e}, \tag{3.6}$$

$$q_e = K_F C_e^n. \tag{3.7}$$

In this equation, q_e (mg/g) represents the amount of Hg^{2+} that is adsorbed once equilibrium is reached. The term q_m (mg/g) indicates the maximum adsorption capacity. K_L (L/mg) is the Langmuir constant, which relates to how strongly the adsorbate binds to the adsorbent. C_e (mg/L) denotes the equilibrium concentration of Hg^{2+} in the solution. Meanwhile, K_F ((mg/g)/(mg/L)^n) and n are Freundlich constants that reflect the adsorption capacity and the intensity of adsorption, respectively.

3.8. Thermodynamic Studies

To reveal the governing mechanism of adsorption, key thermodynamic parameters, including enthalpy change (ΔH), Gibbs free energy (ΔG), and entropy change (ΔS), were evaluated at 293, 303, 313, and 323 K. These parameters provide insight into the spontaneity, heat exchange, and the level of disorder in the adsorption process, thus clarifying whether the adsorption is endothermic or exothermic. Equations 3.8 and 3.9 were used to calculate these parameters:

$$\Delta G = -RT \ln K, \tag{3.8}$$

$$\ln K = -\frac{\Delta H}{RT} + \frac{\Delta S}{R}, \tag{3.9}$$

where R is the universal gas constant (8.314 J/molK), T (K) is the absolute temperature, and K is the equilibrium constant at each respective temperature. The values ΔH, ΔS, and ΔG were computed in kJ/mol, J/molK, and kJ/mol, respectively. By plotting a Van's Hoff plot (*ln K* versus *1/T*), both ΔH and ΔS are determined from the slope and intercept, respectively.

3.9. Desorption Studies

Desorption experiments were conducted to evaluate the reusability of the synthesized pellets for Hg^{2+} ion recovery and to understand the strength of the adsorption mechanism. After adsorption experiments, 1 g of used ABM–PVA pellets were placed in 50 mL of desorbing agents: 0.1-M EDTA and 0.1-M KI. The mixtures were agitated for 24 h at 150 rpm at room temperature (25°C), and the percentage of desorbed Hg^{2+} ions was calculated using Equation 3.10:

$$\%Desorbed = \frac{M_d}{M_a} \times 100, \tag{3.10}$$

where M_d (mg/g) is the amount of desorbed Hg^{2+} and M_a (mg/g) is the amount of adsorbed Hg^{2+}.

CHAPTER FOUR: RESULT AND DISCUSSION

4.1. Characterization

4.1.1. X-ray Fluorescence Spectroscopy

Table 4.1 presents the chemical composition of kaolin before and after treatment. The analysis revealed that silica (49.17%) and alumina (37.5%) are the predominant components in RK, with a minor SO_3 content of 0.04% and CaO content of 0.12%. Following AB treatment, partial dissolution of Al^{3+} and leaching of SO_3 from the octahedral sheet of RK occurred, resulting in an increase in silica content. However, after grafting AB-treated kaolin with 3-MPTS, the SO_3 content rose to 0.16%, and the CaO content reduced to 0.07%, confirming the successful grafting of the 3-MPTS onto the kaolin surface (Pei et al., 2022). The introduction of PVA into the grafted sample did not significantly alter the composition of SO_3 (0.15%). However, compared to ABM, Na_2O and CaO contents increased from 2.807% to 4.532% and 0.071% to 0.133, respectively. This increase is as result of oxygen present, as well as trace metals such as Ca and Na in PVA.

Table 4.1. Chemical composition of RK, AB, ABM, and ABM–PVA

Compound	RK (%)	AB (%)	ABM (%)	ABM–PVA (%)
Na_2O	-	3.441	2.807	4.523
MgO	0.228	0.267	0.188	0.191
Al_2O_3	37.584	27.777	27.993	29.834
SiO_2	49.168	56.060	55.418	50.014
SO_3	0.038	-	0.157	0.146
Cl	0.149	0.837	0.215	0.305
K_2O	1.944	1.818	1.846	1.652
CaO	0.118	0.075	0.071	0.133
TiO_2	0.729	0.839	0.943	0.764
FeO_3	0.902	0.809	0.831	0.776
NiO	0.037	0.025	0.042	0.088
CuO	0.026	0.044	0.034	-
ZnO	-	-	0.033	0.033
Br	7.662	6.747	8.488	10.574
ZrO_2	0.013	0.023	0.025	-
Bi_2O_3	0.135	-	0.171	-
PtO_2	0.572	0.604	-	-
Au	0.603	0.613	0.737	0.906
Nd_2O_3	0.103	-	-	-
Ga_2O_3	-	-	-	0.063

4.1.2. X-ray Diffraction

Figure 4.1 shows the XRD patterns of RK, CK, AB, ABM, and ABM–PVA. For RK, kaolinite and quartz appear as the main crystalline phases. However, once the kaolin is thermally activated (CK), its XRD pattern shows a mostly amorphous structure, which means the characteristic kaolinite peaks are no longer visible (Belver et al., 2002; Zhang et al., 2018). This confirms that the kaolinite has transformed into metakaolinite during thermal treatment. Interestingly, the XRD patterns for AB, ABM, and ABM–PVA look very similar to CK, indicating that the chosen treatments did not considerably change the crystalline structure, but may have modified features such as pore

structure or active sites on the surface (Pei et al., 2022). Nevertheless, slight changes in intensity for some peaks belonging to illite and quartz suggest that the treatments did affect some of the mineral components (Belver et al., 2002).

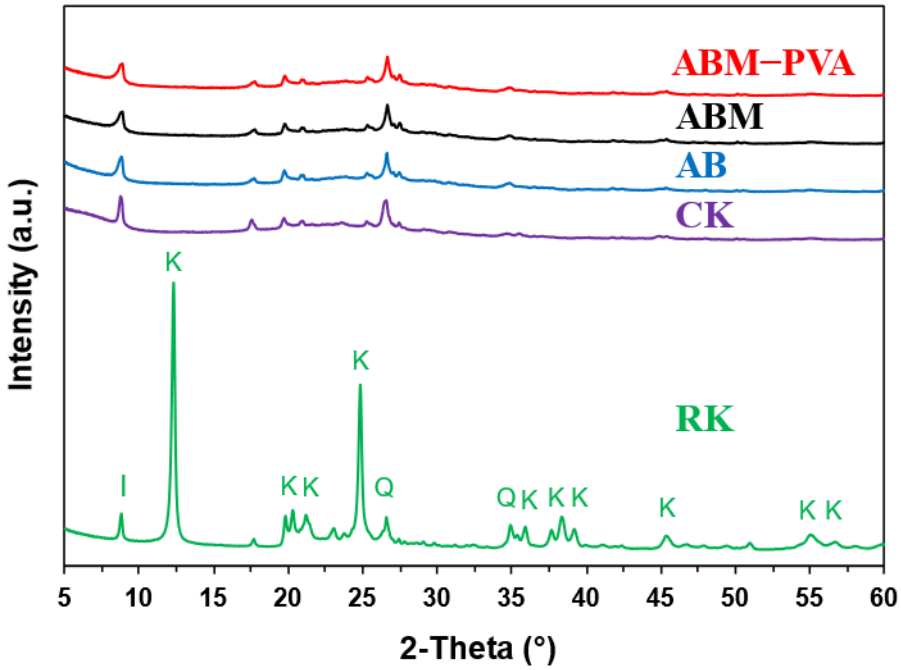

Figure 4.1. XRD patterns of RK, CK, AB, ABM, and ABM–PVA

4.1.3. Fourier Transform Infrared Spectroscopy

Figure 4.2 shows the FTIR spectra of RK, CK, AB, ABM, and ABM–PVA. For RK, notable peaks include 3681 and 3663 cm^{-1} (inner surface OH stretching), as well as 3618 cm^{-1} (inner hydroxyl OH stretching). The band at 1628 cm^{-1} indicates the OH vibration of adsorbed water (Mouni et al., 2018). Moving to the lower wavenumber, the peaks at 1116 and 988 cm^{-1} are attributed to Si–O stretching in quartz, while the peaks at 922 cm^{-1} and 906 cm^{-1} are attributed to the bending (or deformation) of the OH groups on the inner surfaces and within the inner hydroxyl groups (Zhang et al., 2018). In addition, the peaks at 517 cm^{-1} can be linked to the translational movement of the OH groups, whereas the one at 752 cm^{-1} is associated with the bending vibration of the Al–O–Si bonds. However, once RK is converted to CK, the characteristic signals for kaolinite, namely, Al–OH, OH, and Al–O–Si, disappear, leaving a prominent peak at around 1000 cm^{-1} (Si–O stretching). This again confirms the transformation of kaolinite into metakaolinite. From CK onward (i.e., AB, ABM, and ABM–PVA), the FTIR spectra remain consistent, indicating that

these treatments leave the metakaolinite structure largely intact (Pei et al., 2022). These findings align well with the XRD observations in Figure 4.1.

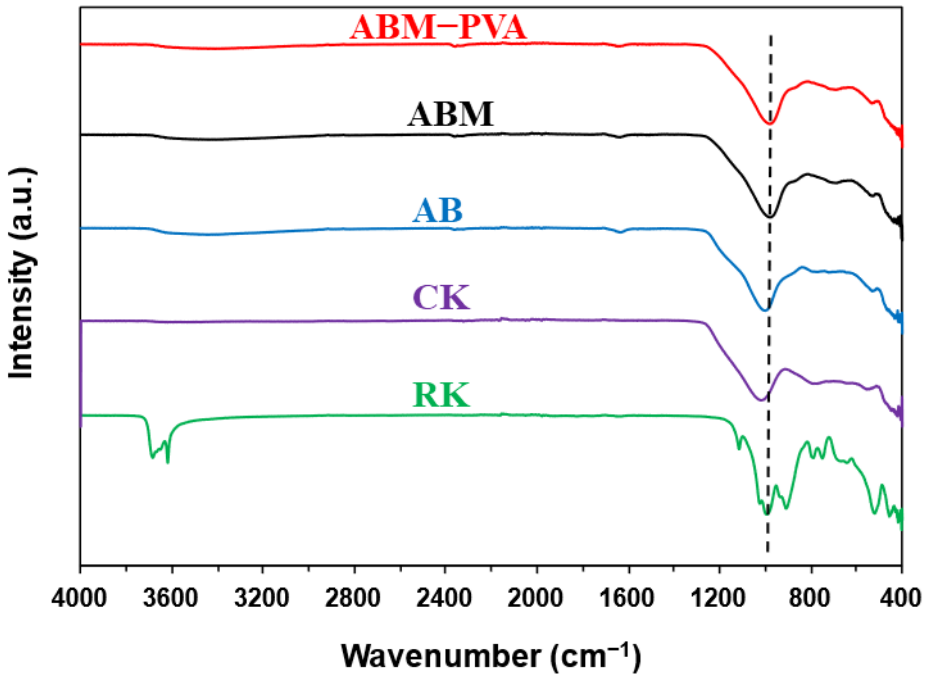

Figure 4.2. FTIR spectra of RK, CK, AB, ABM, and ABM–PVA

4.1.4. Scanning Electron Microscopy–Energy-Dispersive X-ray Spectroscopy

Figures 4.3(a)–4.3(f) show the SEM images of RK, CK, AB, ABM, ABM–PVA, and the developed pellet. SEM image of RK (Figure 4.3(a)) displayed a flake-like structure, which is typical of natural kaolinite (Mouni et al., 2018; Zhang et al., 2018). By contrast, CK (Figure 4.3(b)) exhibited noticeable agglomeration, which can be attributed to the removal of water molecules during thermal activation (Belver et al., 2002). This process results in a reduction in surface area due to the collapse of the kaolinite structure, thereby forming metakaolin. De-agglomeration was observed in AB (Figure. 4.3(c)), which was likely due to the removal of impurities such as Al^{3+} ions, thereby increasing surface area. The pores in ABM (Figure 4.3(d)) appeared closed due to the grafting of 3-MPTS, indicating successful functionalization. Furthermore, ABM–PVA (Figure 4.3(e)) exhibited a smoother surface with a larger cluster of flakes. This is due to the addition of PVA, which serves as a binder during the extrusion process. These morphological changes confirm the progression of structural modifications and successful grafting of the thiol functional groups on the kaolinite surface.

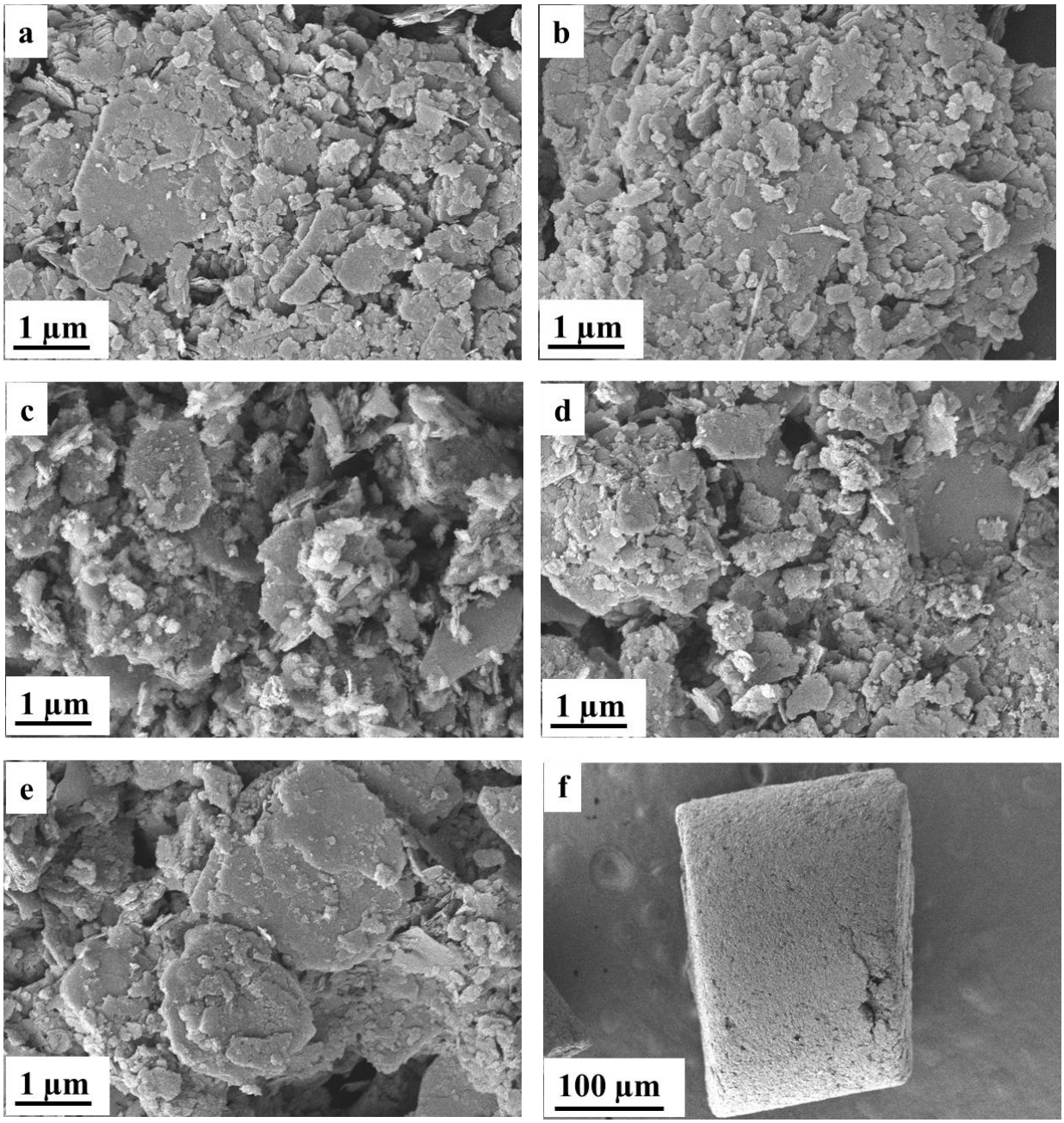

Figure 4.3. SEM images: a) RK, b) CK, c) AB, d) ABM, e) ABM–PVA, and f) developed pellet.

Energy-dispersive X-ray spectroscopy mapping of ABM–PVA pellets was conducted after adsorption to ascertain if mercury was adsorbed onto the surface of the adsorbent. Figure 4.4 shows the EDS mapping confirming the presence of mercury (0.5 wt%) and its successful adsorption. From the figure, it shows that sulfur was insignificant after adsorption. This is due to its formation of a strong bond with mercury, thereby playing a key role by providing extra active

sites. This observation highlights the role of thiol functional groups introduced during grafting in improving the adsorption performance of kaolin.

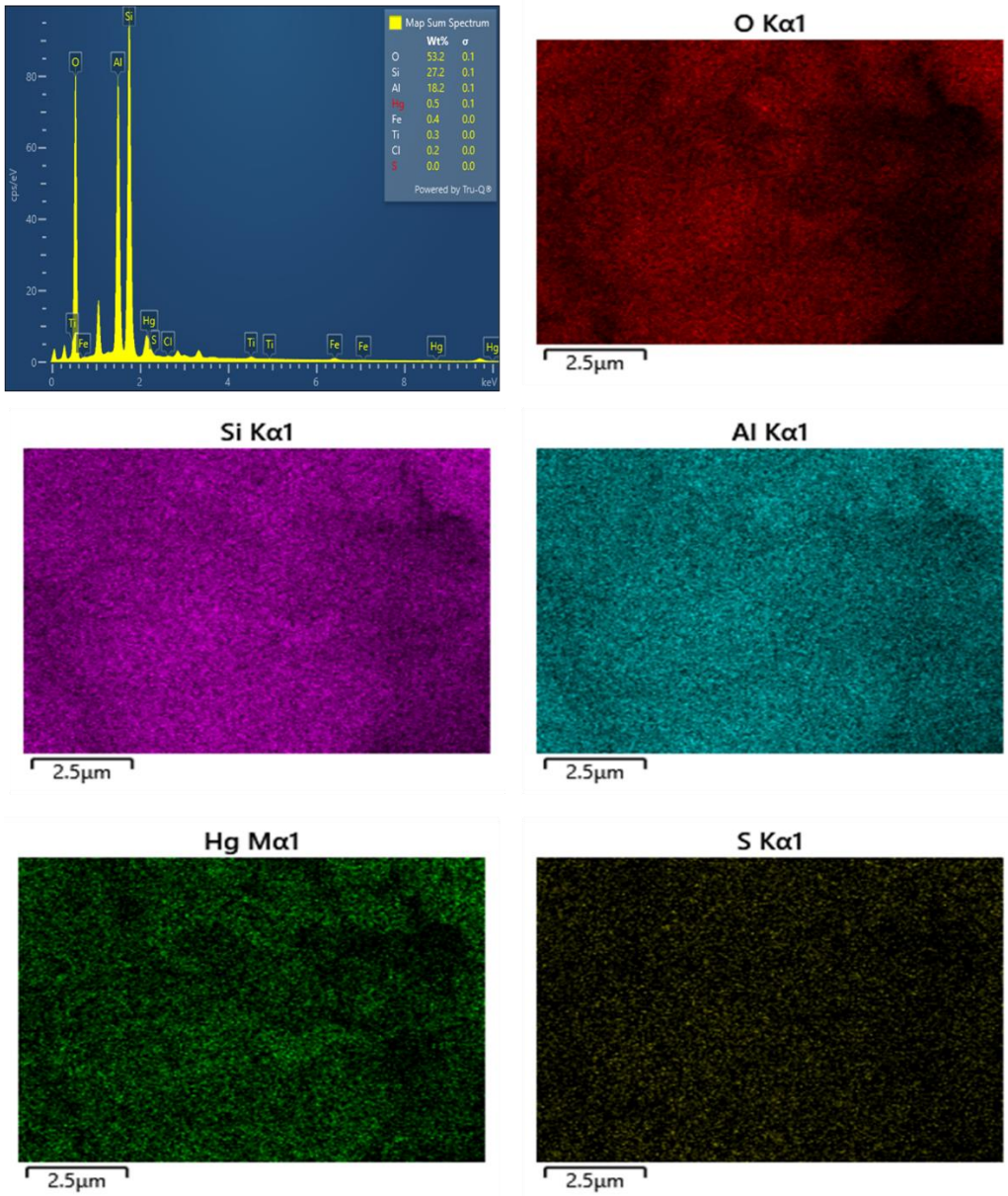

Figure 4.4. EDS mapping of ABM–PVA–Hg

4.1.5. Zeta Potential

Zeta potential was conducted for AB, ABM, and ABM–PVA particles to determine their surface charges. Figure 4.5 shows that the AB, ABM, and ABM–PVA surfaces were all negatively charged between pH 3 and pH 11. The charge on the AB surface ranged from −14.54 mV to −43.52 mV, while ABM ranged from −8.81 mV to −42.56 mV, and ABM–PVA from −10.07 mV to −41.54

mV. The less negative values observed at lower pH suggest protonation of surface functional groups, whereas the increasing negativity at higher pH indicates deprotonation and enhanced surface charge density. This result indicates that since Hg^{2+} is a cationic pollutant, AB, ABM, and ABM–PVA pellets can effectively attract and adsorb it through electrostatic interactions.

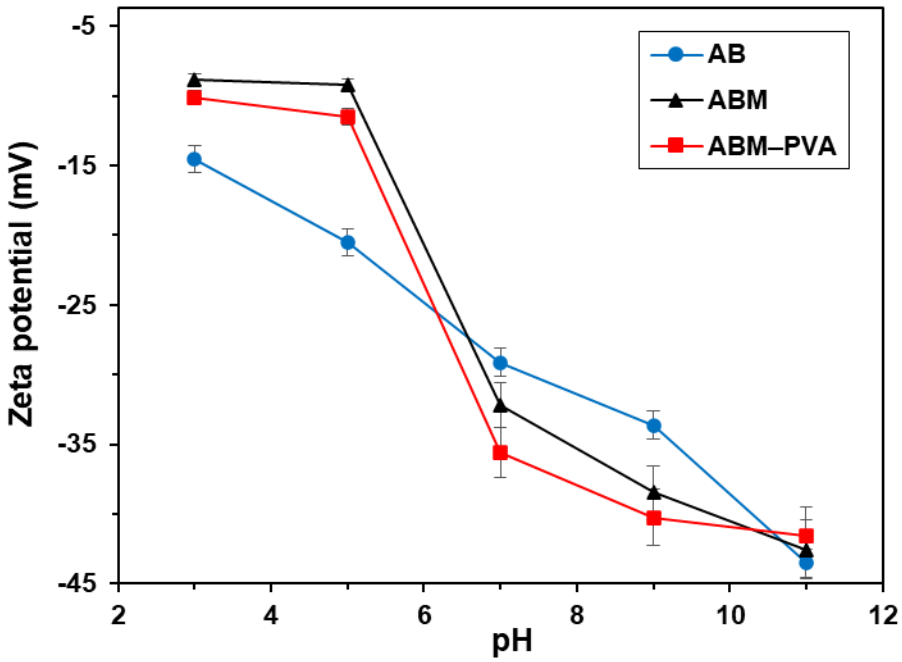

Figure 4.5. Zeta potential of AB, ABM, and ABM–PVA

4.1.6. Brunauer–Emmett–Teller Surface Area Analysis

Table 4.2 presents the surface area, pore volume, and pore diameter of RK, AB, ABM, and ABM–PVA pellets. After AB treatment, the surface area of RK pellets increased more than 4-fold. However, it decreased for ABM and ABM–PVA pellets. This trend was also observed for the pore volume, where RK (0.063 nm) increased significantly after AB treatment (0.222 nm) but decreased to 0.086 and 0.082 nm for ABM and ABM–PVA, respectively. This trend is due to the thiol functional groups filling the pores of ABM and ABM-PVA pellets (Zhang et al., 2018). Pore diameters of RK, AB, ABM, and ABM–PVA pellets were mainly distributed between 6.079 and 16.089 nm, with ABM–PVA pellets being more porous.

Table 4.2. Textural properties of RK, AB, ABM, and ABM–PVA pellets

	RK	AB	ABM	ABM-PVA
Surface area (m^2/g)	16.644	71.516	26.737	20.66
Pore volume (cc/g)	0.063	0.222	0.086	0.082
Pore diameter (nm)	11.68	7.032	6.079	16.089

According to the International Union of Pure and Applied Chemistry (IUPAC), the BET isotherms shown in Figures 4.6(a)–4.6(d) classify RK, AB, ABM, and ABM–PVA pellets as Type IV, with a Type H3 hysteresis loop (Sing et al., 1984; Mustapha et al., 2021). This indicates the presence of slight mesoporous material with small pore sizes.

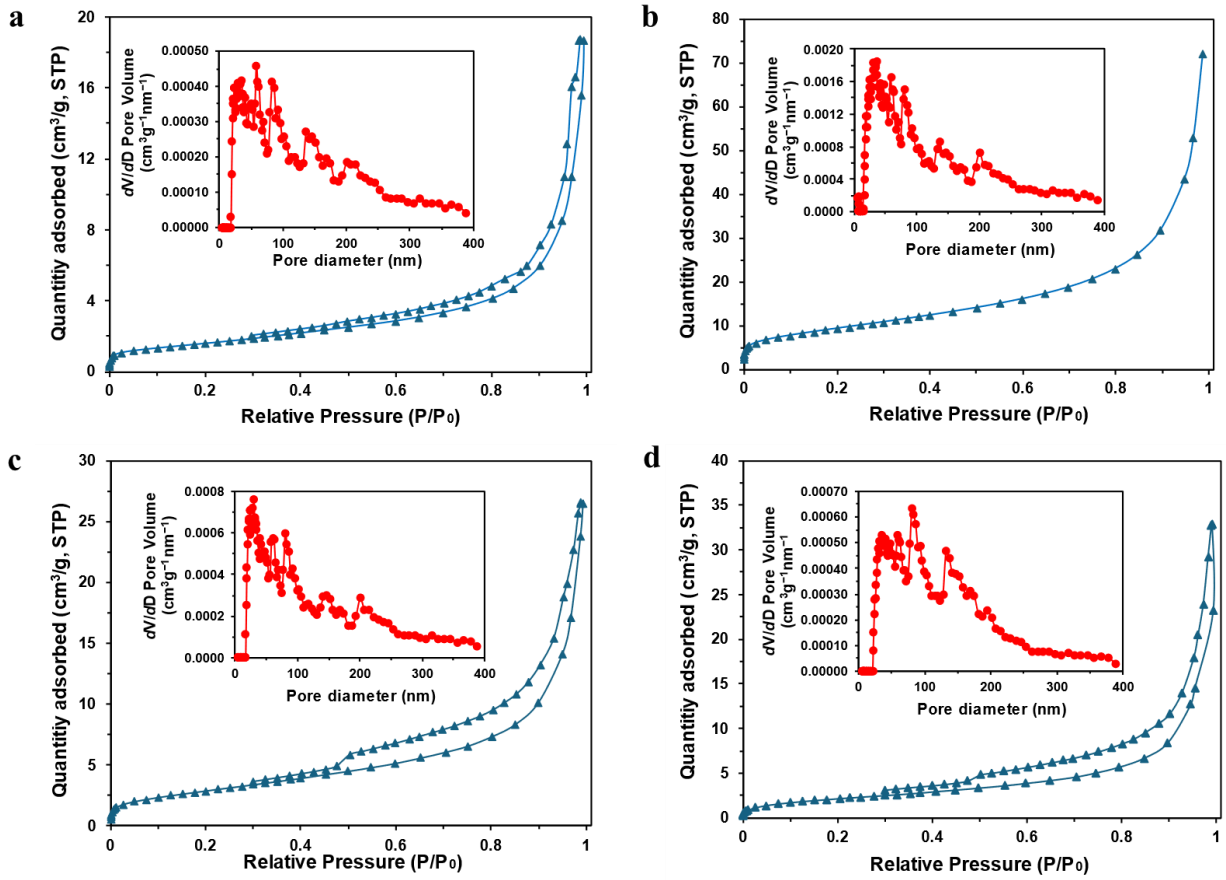

Figure 4.6. Nitrogen adsorption–desorption isotherms and pore diameter distribution (insert): a) RK, b) AB, c) ABM, and d) ABM–PVA pellets.

4.2. Batch Adsorption Studies

4.2.1. Effect of Pellet Size

Figures 4.7 show the influence of pellet sizes on Hg^{2+} adsorption for AB. The 1-mm pellets demonstrated the best performance among the AB pellets, with an adsorption capacity of 4.4 mg/g, followed by the 2-mm pellets (4.1 mg/g) and 3-mm pellets (3.4 mg/g) at an equilibrium time of 120 min. The high adsorption capacity of the 1-mm pellets is attributed to their higher surface area-to-volume ratio compared to the 2- and 3-mm pellets. Additionally, the 1-mm pellets experience a shorter diffusion route, which provides better access to active adsorption sites. By contrast, the 2- and 3-mm pellets experience slower internal diffusion due to their larger volume, therefore limiting their total adsorption rate.

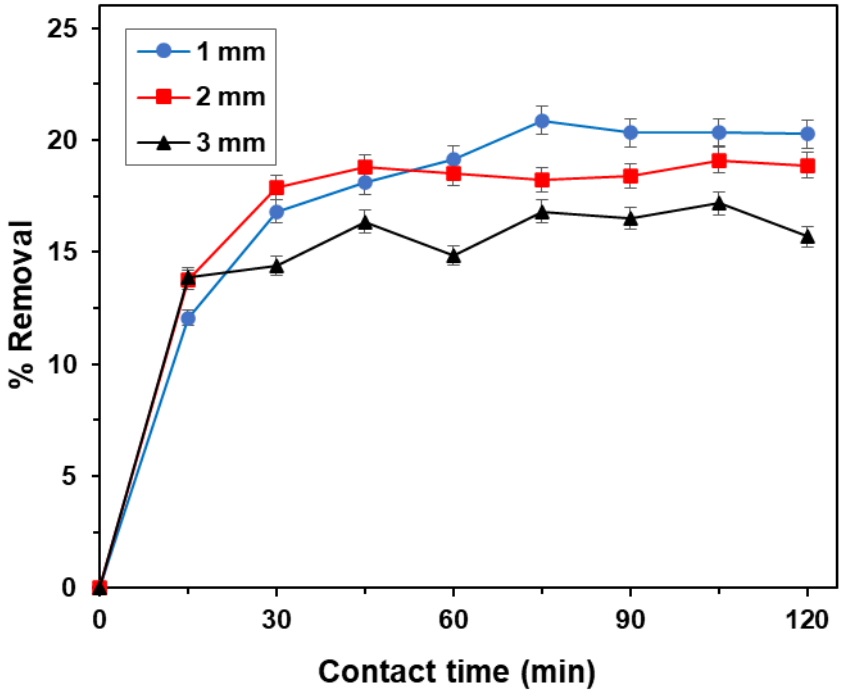

Figure 4.7. Effect of pellet size on AB. Experimental conditions are as follows: C_0 = 50 mg/L; m = 0.5 g; V = 200 mL.

Figure 4.8 presents the effect of pellet sizes on Hg^{2+} adsorption for ABM. Here, the adsorption capacity was observed as 6.6, 7.2, and 5.6 mg/g for 1, 2, and 3 mm pellets, respectively, after an equilibrium time of 240 min, which were higher than those obtained for AB pellets. These higher capacities are due to the thiol functional groups introduced by 3-MPTS grafting. These functional groups formed strong interactions with Hg^{2+} ions compared to the silanol group present in the AB

pellets (Nascimento et al., 2016). Contrary to the AB pellets, which had an optimal performance with I-mm pellets, the best performance for ABM pellets was observed using 2-mm pellets. This is probably because 2-mm pellets ensure better access to thiol functional groups by balancing sufficient surface area and optimal density, thereby enhancing adsorption efficiency. However, due to the denser structure of the 1-mm pellets, it limits the availability of thiol functional groups to Hg^{2+} ions. These findings guided the choice of the 2-mm ABM pellets for further studies due to their remarkable adsorption performance.

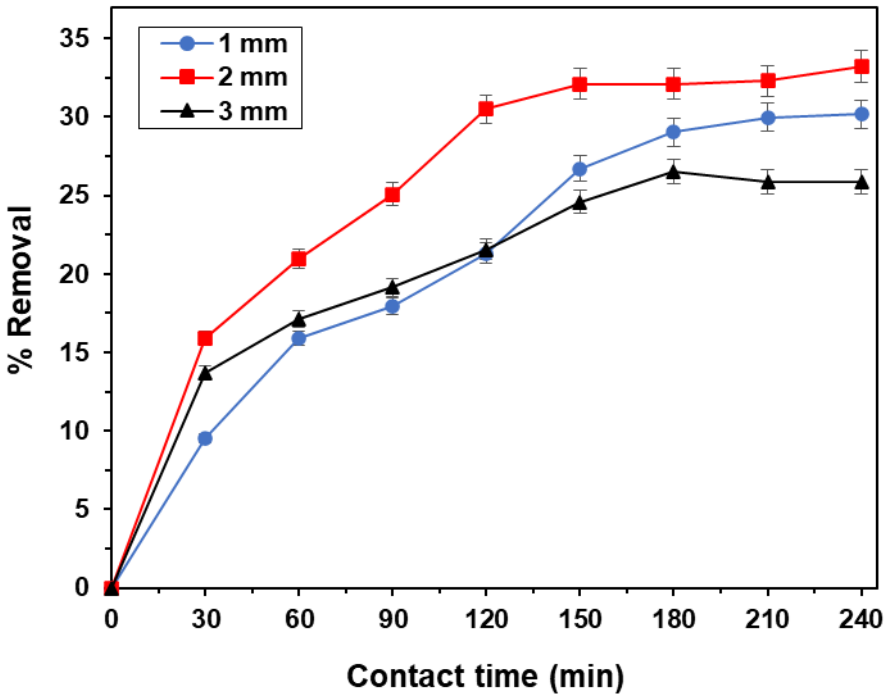

Figure 4.8. Effect of pellet size on ABM. Experimental conditions are as follows: C_0 = 50 mg/L; m = 0.5 g; V = 200 mL.

4.2.2. Effect of Binder Concentration

The effect of binder concentration on the structural integrity of the pellets after adsorption experiments was investigated. As shown in Figure 4.9, varying binder concentrations influenced both Hg removal efficiency and pellet stability after adsorption over an equilibrium time of 48 h. Pellets without binder and those with 0.5 wt% binder achieved Hg removal efficiencies of 40.2% and 38.5%, respectively. However, these pellets exhibited significant weight loss after adsorption, with values of 12.6% and 9.8%, respectively, indicating poor structural integrity. By contrast, pellets containing higher binder concentrations of 1.5, 2.5, and 5 wt% exhibited no observable

weight loss and Hg removal efficiencies of 36.9%, 36.2%, and 34.7%, respectively, demonstrating improved structural integrity and constant efficiency. Among these concentrations, the 1.5 wt% PVA binder provided the optimal balance between structural integrity and adsorption performance, owing to its slightly higher adsorption performance compared to 2.5 and 5 wt% and no weight loss. Based on these findings, 1.5 wt% PVA binder concentration was selected for the preparation of subsequent pellets during the kneading process to ensure both structural integrity and adsorption efficiency.

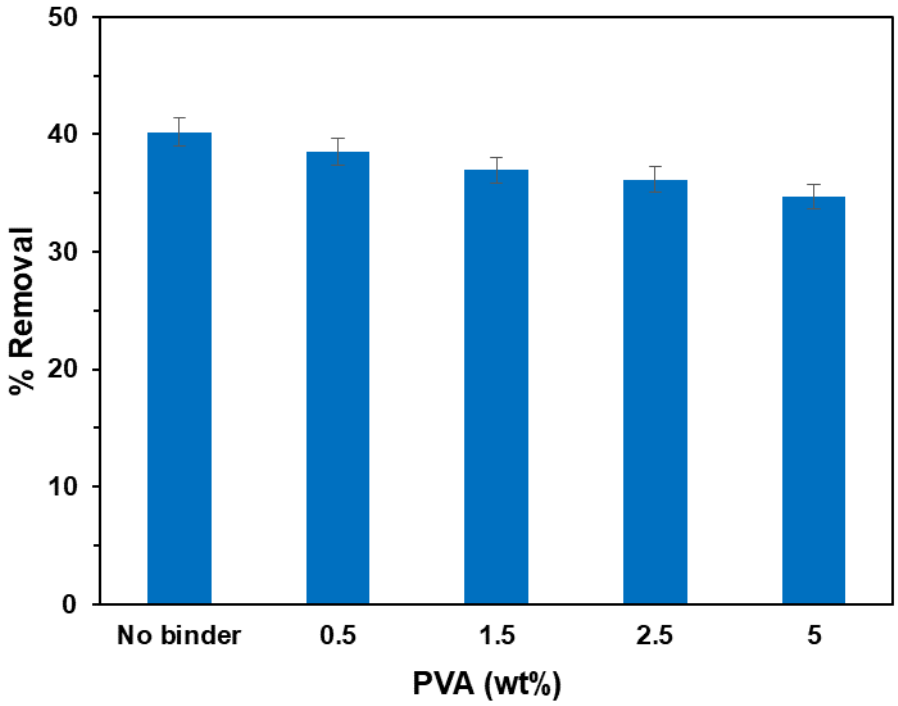

Figure 4.9. Effect of binder concentration. Experimental conditions are as follows: C_0 = 50 mg/L; m = 0.5 g; V = 200 mL.

4.2.3. Effect of Contact Time and Adsorbent Dosage

The effect of contact time and dosage is crucial in order to determine the equilibrium time of adsorption and the maximum removal efficiency of adsorbents. Figure 4.10 shows how contact time and the amount of pellets are influenced by Hg^{2+} adsorption. It was observed that the rate of adsorption increased rapidly from 0 to 6 h for all adsorbent dosages. This increase can be attributed to the availability active sites which are abundant on the surface of the pellets. However, as contact time increased from 6 h to 10 h, the rate of adsorption reduced, indicating that the adsorption process was approaching equilibrium. As contact time increased further to 48 h, the increase in

adsorption was insignificant, indicating that active sites within the pellets were saturated, thereby revealing that equilibrium had been reached. Consequently, equilibrium was obtained after 48 h. Removal efficiency rose from 37.9% to 96.6% when the dosage was increased from 0.5 to 3 g. This can be explained by the readily available binding and exchangeable sites for Hg^{2+} ions (Mustapha et al., 2019). Figure 4.11 shows the corresponding adsorption capacities of the studied dosages. Notably, Hg^{2+} removal at equilibrium was 37.9% and 64.2% for 0.5 and 1g, with adsorption capacities of 7.9 and 6.7 mg/g, respectively. However, for 2 and 3 g, the removal efficiencies were 92.6% and 96.6%, with adsorption capacities of 4.8 and 3.3 mg/g, respectively. The high adsorption capacity observed for both 0.5 and 1 g samples can be attributed to the efficient use of active sites available on the adsorbent. By contrast, the low adsorption capacities at high dosages are probably due to insufficient use of the available active sites, thereby causing site overlapping and agglomeration (Asghar et al., 2023). Thus, 1 g was selected as the optimal dose due to its balance between adsorption capacity and removal efficiency.

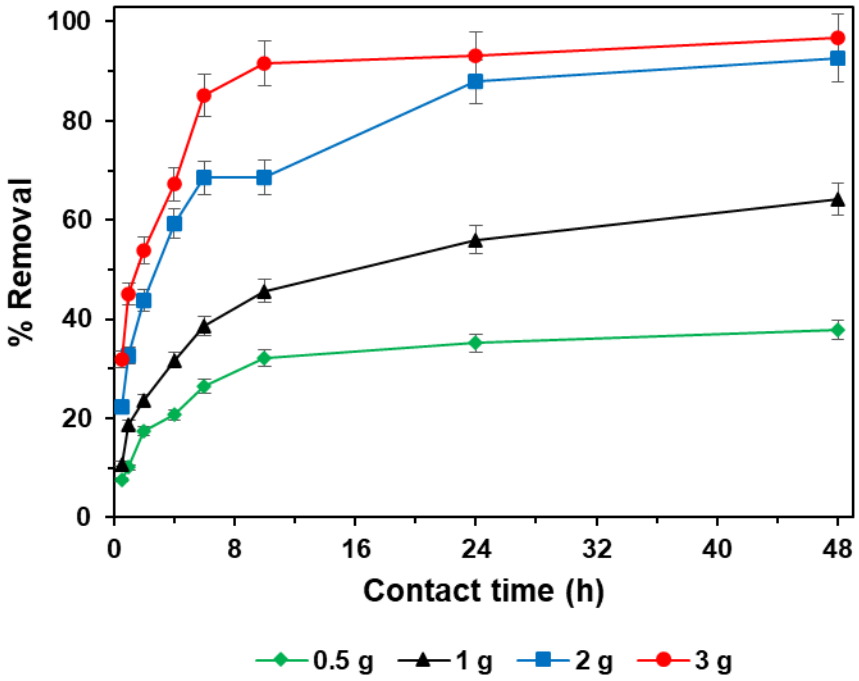

Figure 4.10. Effect of contact time and adsorbent dosage. Experimental conditions are as follows: C_0 = 50 mg/L; V = 200 mL.

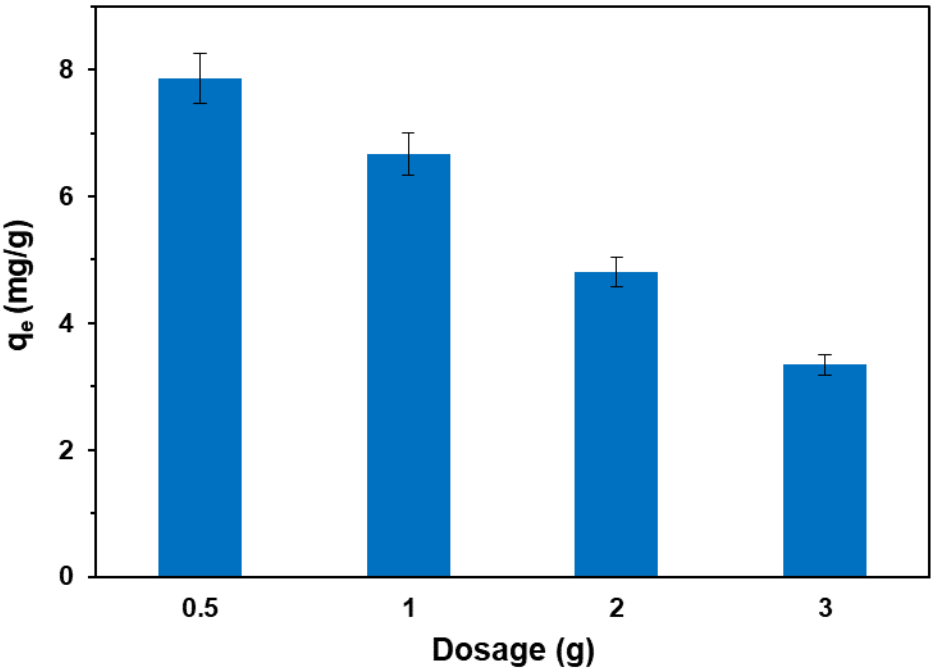

Figure 4.11. Adsorption capacity at varying dosages. Experimental conditions are as follows: C_0 = 50 mg/L; V = 200 mL.

4.2.4. Effect of Solution pH

To assess the influence of pH on Hg^{2+} adsorption, 1 g of ABM–PVA pellets were placed in a 50 mg/L Hg^{2+} solution with different pH at 3, 5, 7, and 9, as shown in Figure 4.12. At equilibrium, adsorption efficiency initially increased as pH increased from 3 to 5 and further decreased as pH increased from 5 to 9. At pH 3, the adsorption efficiency was minimal (54.7%) due to the presence of H^+ and H_3O^+ ions competing for active sites. This partially neutralizes the pellet surface, thereby reducing its net negative charge. At pH 5, the efficiency was optimal. However, at pH 7 and 9, efficiencies were 63.4% and 60.1%, respectively. This decline is attributed to the presence of insoluble, uncharged metal hydroxides, such as $Hg(OH)_2$ (aq), which reduce the electrostatic interaction between Hg^{2+} ions and the adsorbent surface (Huang et al., 2019). The point of zero charge (P_{ZC}) of ABM–PVA pellets was measured at 8.25, as shown in Figure 4.13. This indicates that surface protonation occurs below this pH, reducing Hg^{2+} adsorption via electrostatic attraction. However, at pH values above P_{ZC}, surface deprotonation occurs, increasing electrostatic attraction thereby enhancing adsorption. Adsorption in these systems was not governed solely by electrostatic interactions; however, other mechanisms, such as chemosorption and surface

complexation, also contribute substantially. Therefore, pH 5 was chosen as the optimal pH because it maximizes negative surface charge while minimizing interference from competing protons or hydroxide precipitation.

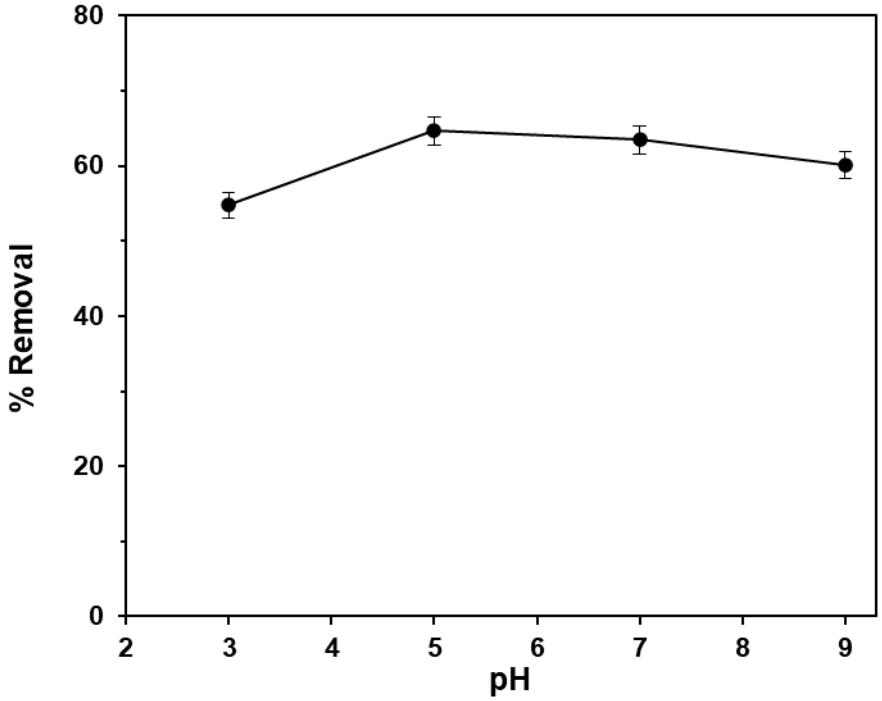

Figure 4.12. Effect of solution pH. Experimental conditions are as follows: C_0 = 50 mg/L; m = 1 g; V = 200 mL.

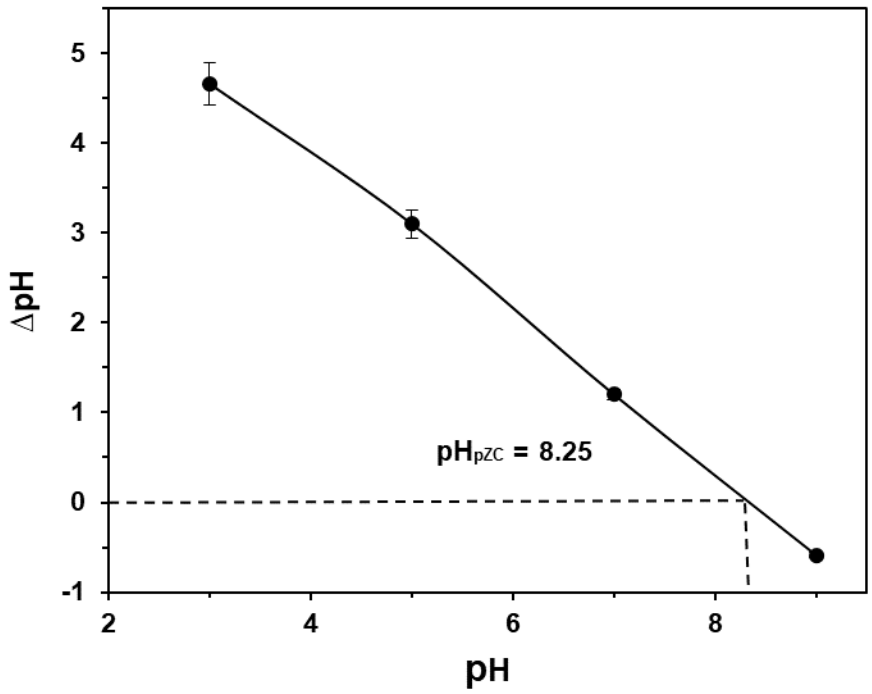

Figure 4.13. Point of zero charge of ABM–PVA pellets

4.2.5. Effect of Initial Concentration

Effect of initial concentration was investigated to determine the optimal concentration to maximize the utilization of active sites. As shown in Figure 4.14, adsorption capacity increased as the initial concentration increased from 25 mg/L to 100 mg/L but plateaus at 100 mg/L. This is because, at lower concentrations (25 mg/L), the driving force for mass transfer is low, implying that despite the availability of active sites, only fewer molecules can occupy active sites. By contrast, at higher concentrations (50 and 75 mg/L), the adsorbent reached saturation rapidly due to more molecules occupying active sites. Further increase in initial concentration (100 and 125 mg/L) led to a plateau, indicating that equilibrium has been attained. Therefore, the optimal initial concentration was 100 mg/L.

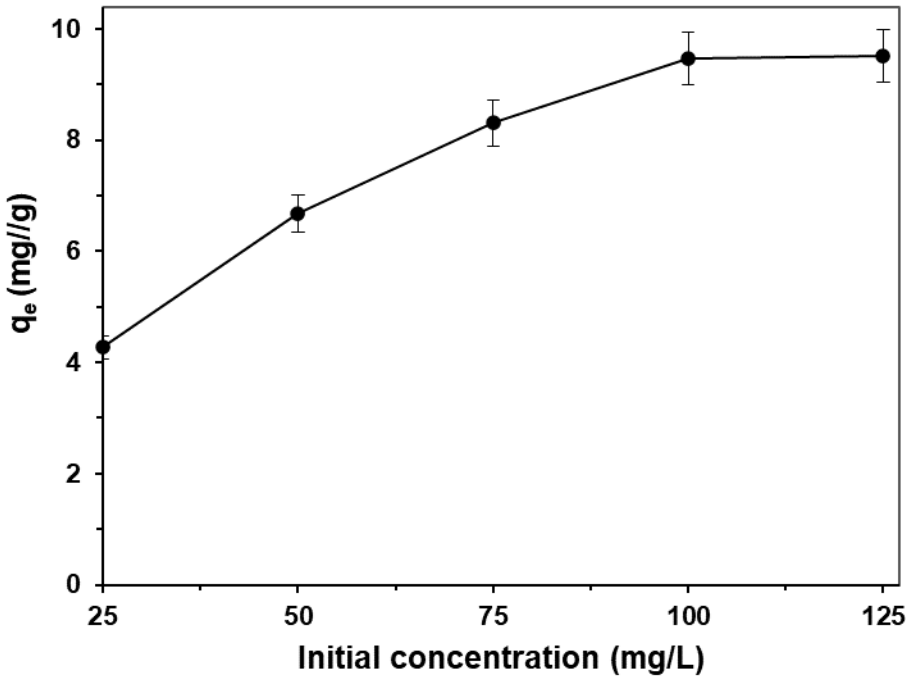

Figure 4.14. Effect of initial concentration. Experimental conditions are as follows: m = 1 g; pH = 5; V = 200 mL.

4.2.6. Effect of Temperature

Effect of temperature plays a crucial role in determining whether the adsorption process is favored by the endothermic or exothermic reaction. Figure 4.15 shows the effect of temperature on Hg^{2+} adsorption onto AMB–PVA pellets by varying temperature from 20°C to 50°C. Adsorption efficiency increased (64.2% to 79.1) with an increase in temperature, implying that the adsorption process is endothermic. For an endothermic adsorption process, a higher temperature provides the energy required to overcome activation barriers associated with chemical interactions, such as surface complexation or chemosorption. This indicates that surface complexation or chemosorption might be one of the mechanisms occurring during the adsorption of Hg^{2+} adsorption onto AMB–PVA pellets.

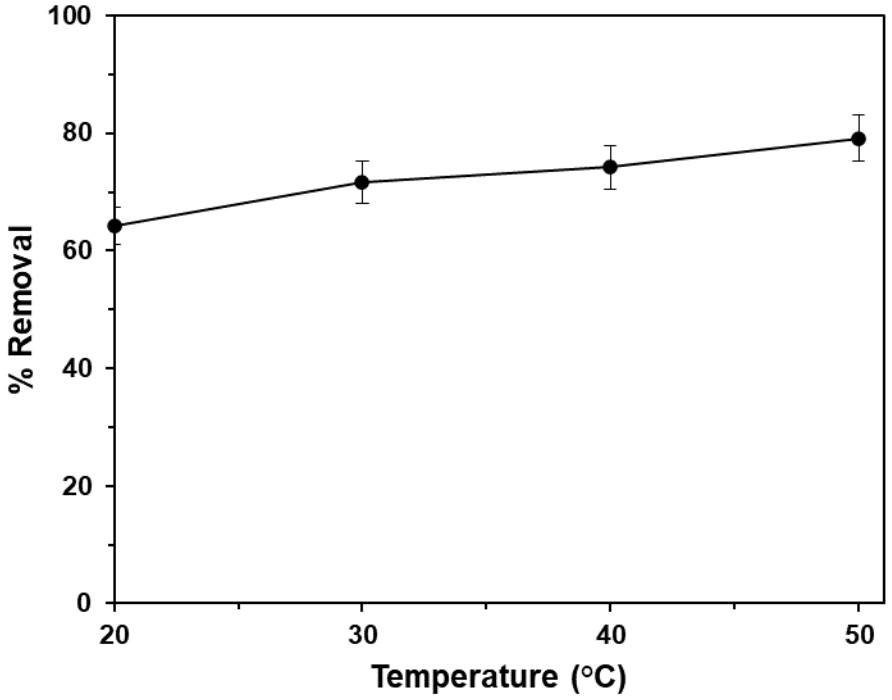

Figure 4.15. Effect of temperature. Experimental conditions are as follows: C_0 = 50 mg/L; m = 1 g; V = 200 mL.

4.3. Kinetics Studies

Figure 4.16 illustrates the fitting of PFO and PSO kinetic models to the experimental data for Hg^{2+} adsorption onto ABM–PVA pellets, with the corresponding fitting parameters detailed in Table 4.3. The PSO model provided an excellent fit, with correlation coefficients (R^2) and sum of squared error (SSE) of 0.986 and 0.626, respectively, outperforming the PFO model ($R^2 \approx 0.963$; SSE ≈ 1.906). This agrees with Simonin's survey, which states that PSO usually yields higher R^2 than PFO in adsorption studies (Simonin, 2016). Moussout et al. (2018) likewise observed that PSO offers superior correlation (often $R^2 \approx 1$) and recommended using both R^2 and error metrics to judge kinetic fits. In this study, the PSO fit not only has a higher R^2 but also a much lower SSE, indicating a more accurate representation of the uptake rate. Similar trends have been reported for Hg^{2+} adsorption onto clays. For instance, Pie et al. (2022) report that Hg^{2+} sorption kinetics conform to PSO with high R^2 and rapid initial uptake rates, which is consistent with chemisorptive surface interactions. Notably, a polypyrrole–Fe_3O_4/kaolin composite achieved R^2 of 0.966 for PFO and 0.983 for PSO when employed for Hg^{2+} removal (Lin et al., 2020), confirming the better performance of the PSO model. The superior performance of PSO is often interpreted as evidence

that chemisorption controls the rate (since chemical bonding or electron sharing is the rate-limiting step). In this study, the kinetic data (better PSO fit) coupled with other findings, such as the SSE, strongly suggest that chemisorptive interactions play a major role in Hg^{2+} uptake.

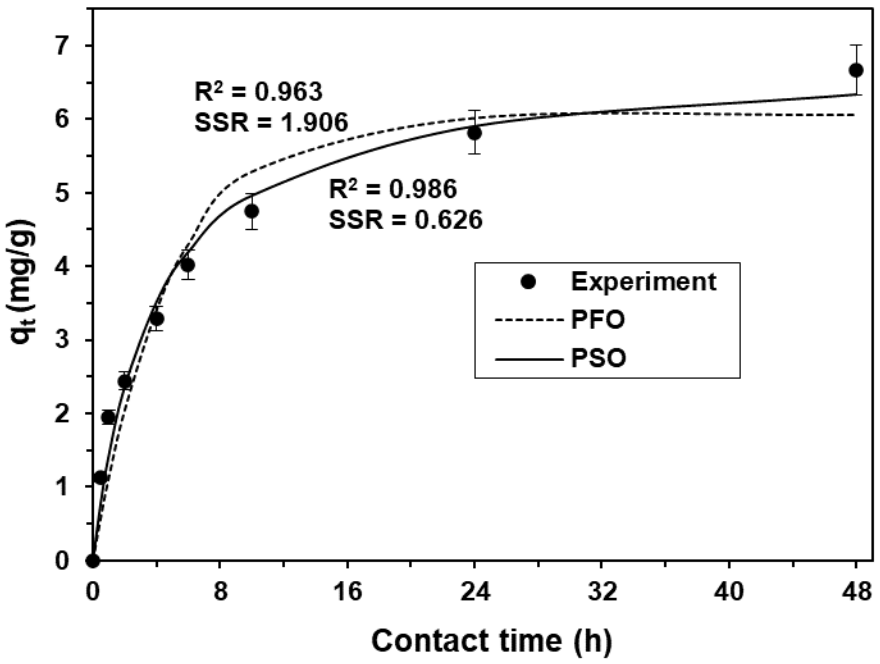

Figure 4.16. Adsorption kinetics of ABM–PVA pellets. Experimental conditions are as follows: C_0 = 50 mg/L; m = 1 g; V = 200 mL.

Table 4.3. Fitting parameters for PFO and PSO kinetic models

Kinetics	Parameter	Value
Pseudo-first order	K_1	0.21
	q_m	6.06
	R^2	0.963
	SSE	1.906
Pseudo-second order	K_2	0.04
	q_m	6.84
	R^2	0.986
	SSE	0.626

4.4. Isotherm Studies

Figures 4.17 and 4.18 present the Langmuir and Freundlich isotherms, respectively, at temperatures of 293, 303, and 313 K, with their fitting parameters summarized in Table 4.4. The Freundlich model provided an excellent fit with R^2 values of 0.987–0.997. This suggests adsorption on a heterogeneous surface with multiple energy sites (Freundlich, 1907). By contrast, the Langmuir model yielded monolayer capacities, q_m, of 10.1–12.5 mg/g (in the 293–313 K range) for the pellets, indicating the process is temperature-dependent. These capacities are quite low compared to other functionalized clay. For instance, Pie et al. (2022) noted a q_m of 26.21 and 30.83 mg/g for functionalized montmorillonite for the immobilization of Hg^{2+}. In fact, Lin et al. (2020) noted a q_m of 471.2 mg/g at 298 K, rising to 633.8 mg/g at 318 K when polypyrrole/Fe_3O_4-coated kaolin was used for Hg^{2+} uptake. The reason for the discrepancies in q_m for this study and other studies may be due to the pelleting process, which can reduce the effective surface area and accessibility of active sites, as opposed to powdered forms of clay or composites, which often have a greater surface area available for adsorption. In addition, by creating a pelleted structure, pore blockage or diffusion limitations may arise, especially if the pore openings are constricted during pellet formation. Consequently, though the ABM–PVA pellets display a strong affinity for mercury ions, the net adsorption capacity is limited by these physical and chemical constraints. Overall, the temperature dependence, combined with the strong fit of the Freundlich model, reinforces the notion of a heterogeneous and endothermic adsorption mechanism. The endothermic nature is likely due to chemisorption, wherein the energy barrier for forming covalent bonds with thiol groups is overcome at higher temperatures.

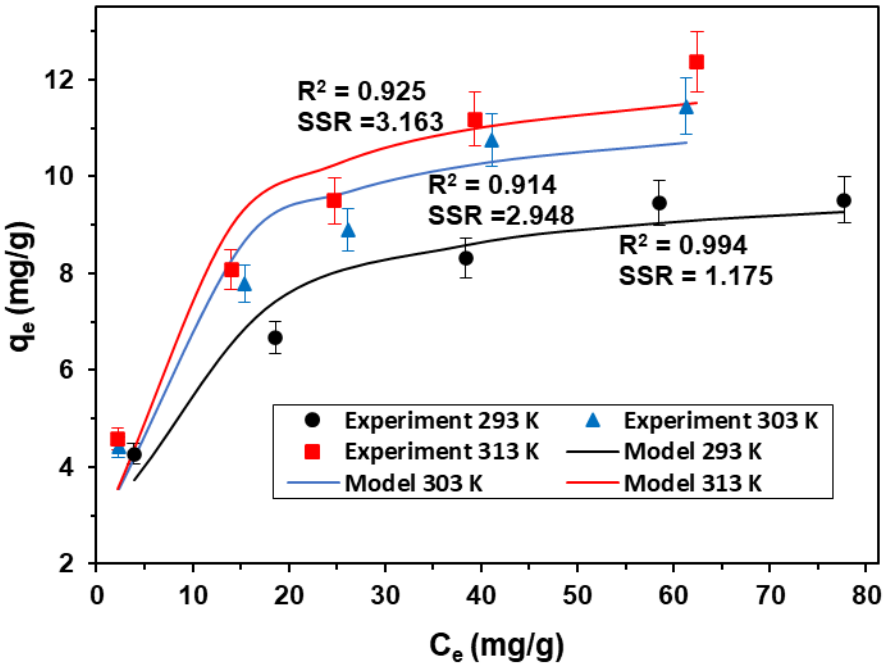

Figure 4.17. Langmuir model. Experimental conditions are as follows: C_0 = 50 mg/L; m = 1 g; V = 200 mL.

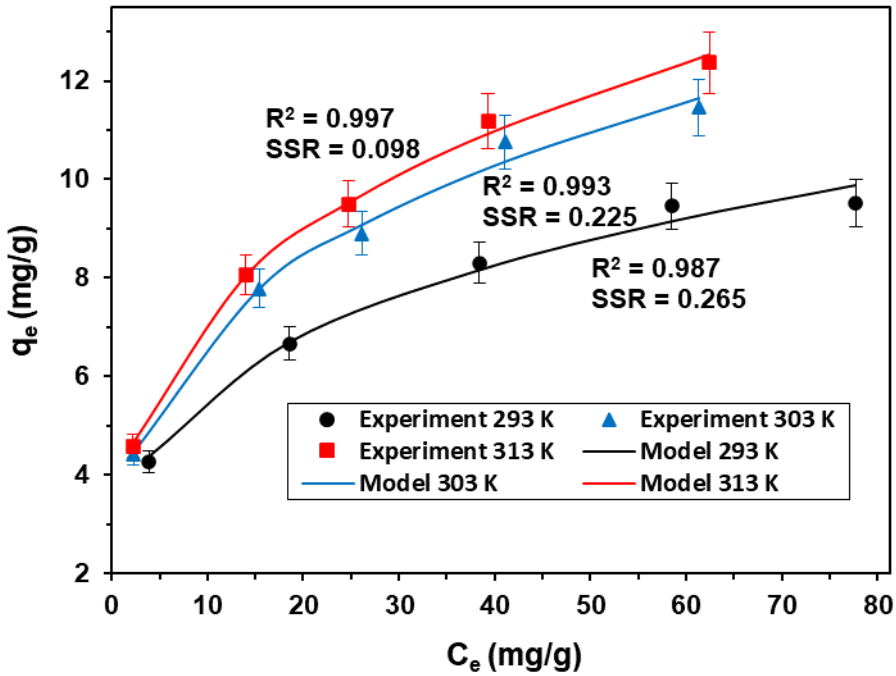

Figure 4.18. Freundlich model. Experimental conditions are as follows: C_0 = 50 mg/L; m = 0.5 g; V = 200 mL.

Table 4.4. Adsorption isotherm fitting parameters

Isotherm	Parameter	Value		
		293 K	303 K	313 K
Langmuir	q_m	10.06	11.62	12.55
	R^2	0.944	0.914	0.925
	K_L	0.152	0.193	0.179
	SSE	1.175	2.948	3.163
Freundlich	*n*	0.271	0.294	0.296
	R^2	0.987	0.993	0.997
	K_F	3.03	3.48	3.68
	SSE	0.265	0.225	0.098

4.5. Thermodynamics Studies

Thermodynamic studies were conducted to gain more insight into the mechanism governing the adsorption process. Figure 4.19 presents the van't Hoff plot, from which the ΔH was determined as 18.8 kJ/mol and ΔS was 55.7 J/(mol·K). The positive ΔH confirms that the adsorption is endothermic, whereas increasing disorder at the interface of the sorbate and sorbent indicates a positive ΔS (Mustapha et al., 2021). The values for ΔG at 293, 303, 313, and 323 K were −16.3, −16.9, −17.4, and −18.0, respectively. The negative ΔG values observed at all temperatures indicate that the adsorption process happens spontaneously under the different conditions. Additionally, it appears that ΔG values become less negative with rising temperature, suggesting that higher temperatures slightly reduce the spontaneity. Therefore, these results suggest that chemisorption was the dominant mechanism during the adsorption process, involving stronger interactions such as covalent bonding between the thiol functional groups and Hg^{2+}.

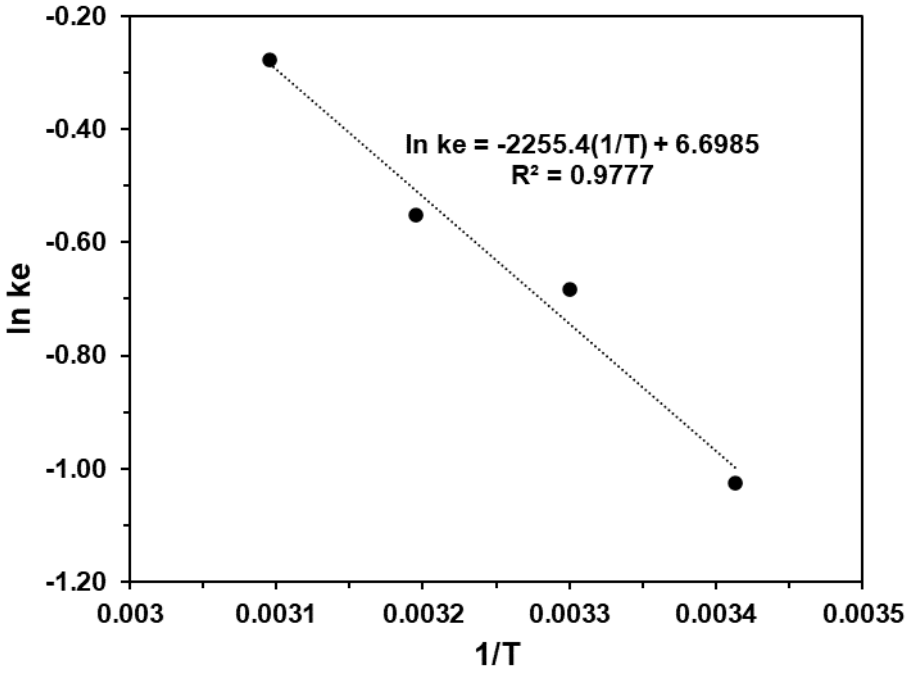

Figure 4.19. van't Hoff plot used to determine ΔH and ΔS

4.6. Desorption Studies

To explore how reversible the adsorption of Hg^{2+} is and how strongly it binds to functional groups on the adsorbent surface, desorption of Hg^{2+} ions from ABM–PVA pellets was conducted using EDTA and KI. As shown in Figure 4.20, desorption efficiencies were 4.1% and 3.8% for EDTA and KI, respectively, after 1 h. After 4 h, the desorption efficiencies increased to 8.1% for EDTA and 7.5% for KI. This low desorption performance likely stems from Hg^{2+} binding tightly to thiol functional groups on the pellet surface, thereby forming strong bonds that resist being broken apart (Nascimento et al., 2016). However, after 24 h, desorption efficiency increased to 50.8% for EDTA and 44.3% for KI. This increase suggests that, over time, the desorbing agents chelate other functional sites, such as silanol and aluminol groups, which form weak bonds. These results show the dual mechanism of Hg^{2+} binding on the surface of ABM–PVA pellets: an initial, stronger contact with thiol functional groups and a much weaker reversible binding with silanol and aluminol groups.

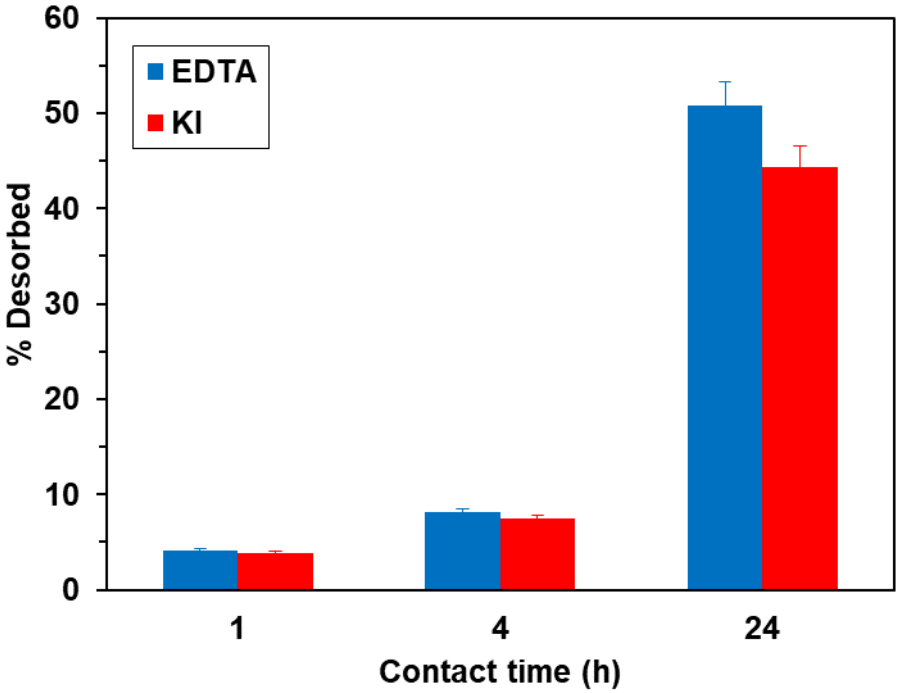

Figure 4.20. Desorption efficiency of ABM–PVA pellets

CHAPTER FIVE: CONCLUSION

5.1. Thesis Summary

This thesis explored the potential of kaolin pellets, synthesized through sequential chemical treatments, as an efficient and cost-effective for mercury removal from contaminated water. Initially, treatment methods, such as thermal activation and acid–base treatments, were conducted to enhance the adsorption performance of kaolin. Grafting of 3-MPTS was further performed to introduce thiol functional groups, which markedly strengthened the adsorbent's affinity for Hg^{2+} ions. An extrusion process with PVA as a binder was employed to transform the modified kaolin into mechanically stable pellets suitable for industrial-scale operations. Comprehensive adsorption studies were then performed, focusing on the effect of pellet size, contact time, adsorbent dosage, pH, temperature, and initial concentration. The main findings of this research are summarized as follows:

- Grafting thiol functional groups onto the kaolin surface by 3-MPTS resulted in robust chemical bonds with Hg^{2+} ions. The introduction of thiol functional groups thus substantially boosted adsorption performance relative to acid–base treated kaolin pellets.

- Kaolin powder was successfully extruded into cylindrical pellets of 1–3 mm diameter. The addition of 1.5% (w/w) PVA as a binder imparted high mechanical strength, minimizing breakage during extended contact with mercury-contaminated solutions. Pellets in the 2 mm size range achieved the best performance due to better access to thiol functional groups by balancing sufficient surface area and optimal density.

- Batch adsorption experiments showed that optimal mercury removal was achieved at pH 5 when 1 g of adsorbent was added to 200 mL of a 50 mg/L mercury solution, reaching equilibrium in ~48 h. The adsorption capacity and percentage removal at these conditions are 6.7 mg/g and 64.2%, respectively.

- Adsorption kinetics followed a PSO model, indicating that chemisorption is the dominant mechanism. Importantly, adsorption isotherms were employed to further understand the interaction between mercury and the adsorbent surface. The Freundlich isotherm model

provided a superior fit to the experimental data compared to the Langmuir model, as evidenced by higher correlation coefficients (R^2 values of 0.987–0.997). Meanwhile, the Langmuir model yielded maximum adsorption capacities that increased with temperature (10.06–12.55 mg/g), highlighting the temperature-dependent nature of the process. Thermodynamic parameters ($\Delta H = 18.8$ kJ/mol; $\Delta S = 55.7$ J/molK; negative ΔG) confirmed an endothermic and spontaneous process, highlighting the viability of operating at higher temperatures to increase uptake rates.

- Desorption studies using EDTA and KI revealed partial reversibility, suggesting that mercury forms stable surface complexes with the thiol functional groups present in the adsorbent. While this strongly secures mercury in the adsorbent and reduces the risk of recontamination, it also limits the ease of adsorbent regeneration.

Overall, this thesis demonstrated that thiol-functionalized, pelletized kaolin is a practical and efficient adsorbent for mercury removal. It exhibits strong bonding with mercury, minimal generation of harmful by-products, and robust mechanical stability, which are critical attributes for industrial wastewater treatment. Additionally, given that Kazakhstan has abundant kaolin deposits and substantial industrial activities, particularly in mining and oil and gas regions such as Pavlodar, this technology presents a promising solution for mitigating mercury contamination in local water resources.

5.2. Future Work

Future research may extend this research by investigating alternative acid–base treatments, refining binder formulations for enhanced pellet durability, and optimizing regeneration methods, thereby further establishing kaolin pellets as a sustainable solution for mercury and other heavy-metal contaminants. Additionally, future studies should investigate the performance of functionalized kaolin pellets in large-scale columns and packed-bed reactors, with a focus on optimizing operational parameters including column and height flow rate to maintain high mercury removal efficiency.

REFERENCES

Ahamad, M. I., Yao, Z., Ren, L., Zhang, C., Li, T., Lu, H., ... & Feng, W. (2024). Impact of heavy metals on aquatic life and human health: a case study of River Ravi Pakistan. Frontiers in Marine Science, 11, 1374835. https://doi.org/10.3389/fmars.2024.1374835

Ahmad, N. I., Mahiyuddin, W. R. W., Azmi, W. N. F. W., Azlee, R. S. R., Shaharudin, R., & Sulaiman, L. H. (2022). Exposure Assessment of methyl mercury from consumption of fish and seafood in Peninsular Malaysia. *Environmental Science and Pollution Research*, *29*(17), 24816-24832. https://doi.org/10.1007/s11356021-17483-6

Akhtar, A., Kazi, T. G., Afridi, H. I., Baig, J. A., Musharraf, S. G., & Arain, M. B. (2021). Efficiency of different green shaking extraction methods for the preconcentration of trace quantity of mercury in artificial saliva extract of snuff products: impact on adult consumers. *Chemical Papers*, 75, 3005-3015. https://doi.org/10.1007/s11696-021-01545-7

Alali, J. M. (2020). Beneficiation of White Kaolinitic Sandstone to Produce Kaolin Concentrate from Wadi Siq-Rakyia Area in Wadi Araba, Jordan. *Open Journal of Geology*, 10(08), 829. https://doi.org/10.4236/ojg.2020.108037

Al-Ghouti, M. A., Da'ana, D., Abu-Dieyeh, M., & Khraisheh, M. (2019). Adsorptive removal of mercury from water by adsorbents derived from date pits. *Scientific reports*, 9(1), 15327. https://doi.org/10.1038/s41598-019-51594-y

Al-Sulaiti, M. M., Soubra, L., & Al-Ghouti, M. A. (2022). The causes and effects of mercury and methylmercury contamination in the marine environment: A review. Current Pollution Reports, 8(3), 249-272. https://doi.org/10.1007/s40726-022-00226-7

Altunkaynak, Y., Canpolat, M., & Yavuz, Ö. (2024). Adsorption of mercury (II) ions on kaolinite from aqueous solutions: Isothermal, kinetic, and thermodynamic studies. *Environmental Progress & Sustainable Energy*, 43(2), e14295. https://doi.org/10.1002/ep.14295

Anagho, S. G., Ketcha, J. M., Tchuifon, T. D. R., & Ndi, J. N. (2013). Kinetic and equilibrium studies of the adsorption of mercury (II) ions from aqueous solution using kaolinite and metakaolinite clays from Southern Cameroon. *International Journal of Research in Chemistry and Environment*, 3(2), 1-11.

Aqdam, M. M., Baltzer, J. L., Branfireun, B. A., Low, G., Low, M., & Swanson, H. K. (2024). Can remotely sensed catchment to lake area ratios predict mercury levels in subarctic fishes?. Environmental Research, 260, 119545. https://doi.org/10.1016/j.envres.2024.119545

Arayachukiat, S., Pironchart, T., & Kongpatpanich, K. (2022). The Versatile and Tunable Metal-Organic Framework MOF for Condensate Decontamination. In *Offshore Technology Conference Asia* (p. D041S038R002). OTC. https://doi.org/10.4043/31664-MS

Arif, M., Liu, G., Yousaf, B., Ahmed, R., Irshad, S., Ashraf, A., ... & Rashid, M. S. (2021). Synthesis, characteristics and mechanistic insight into the clays and clay minerals-biochar

surface interactions for contaminants removal-A review. *Journal of Cleaner Production*, 310, 127548. https://doi.org/10.1016/j.jclepro.2021.127548

Asghar, S., Roudgar-Amoli, M., Alizadeh, A., & Shariatinia, Z. (2023). Water Purification Through Adsorption of Organic Pollutant onto Novel and Effective Phosphorus-Containing g-C3N4/FeMo0.5O3 Nanocomposites. Water, Air, and Soil Pollution, 234(1). https://doi.org/10.1007/s11270-023-06065-6

Balali-Mood, M., Naseri, K., Tahergorabi, Z., Khazdair, M. R., & Sadeghi, M. (2021). Toxic mechanisms of five heavy metals: mercury, lead, chromium, cadmium, and arsenic. Frontiers in pharmacology, 12, 643972. https://doi.org/10.3389/fphar.2021.643972

Barakan, S., & Aghazadeh, V. (2021). The advantages of clay mineral modification methods for enhancing adsorption efficiency in wastewater treatment: a review. Environmental Science and Pollution Research, 28(3), 2572-2599. https://doi.org/10.1007/s11356-020-10985-9

Barone, G., Storelli, A., Meleleo, D., Dambrosio, A., Garofalo, R., Busco, A., & Storelli, M. M. (2021). Levels of mercury, methylmercury and selenium in fish: insights into children food safety. Toxics, 9(2), 39. https://doi.org/10.3390/toxics9020039

Bazargan, A., Hadi, P., Rough, S. L., & McKay, G. (2016). The preparation of pellets by the compaction of an aluminosilicate-based adsorbent from electronic waste. Journal of environmental chemical engineering, 4(2), 2322-2326. https://doi.org/10.1016/j.jece.2016.03.047

Belver, C., Bañares Muñoz, M. A., & Vicente, M. A. (2002). Chemical activation of a kaolinite under acid and alkaline conditions. Chemistry of materials, 14(5), 2033-2043. https://doi.org/10.1021/cm0111736

Benalia, M. C., Youcef, L., Bouaziz, M. G., Achour, S., & Menasra, H. (2022). Removal of heavy metals from industrial wastewater by chemical precipitation: mechanisms and sludge characterization. Arabian Journal for Science and Engineering, 47(5), 5587-5599. https://doi.org/10.1007/s13369-021-05525-7

Bjørklund, G., Chirumbolo, S., Dadar, M., Pivina, L., Lindh, U., Butnariu, M., & Aaseth, J. (2019). Mercury exposure and its effects on fertility and pregnancy outcome. *Basic & clinical pharmacology & toxicology*, *125*(4), 317-327. https://doi.org/10.1111/bcpt.13264

Cardoso, S. P., Faria, T. L., Pereira, E., Portugal, I., Lopes, C. B., & Silva, C. M. (2020). Mercury removal from aqueous solution using ETS-4 in the presence of cations of distinct sizes. *Materials*, 14(1), 11. https://doi.org/10.3390/ma14010011

Chojnacki, A., Chojnacka, K., Hoffmann, J., & Gorecki, H. (2004). The application of natural zeolites for mercury removal: from laboratory tests to industrial scale. *Minerals Engineering*, 17(7-8), 933-937. https://doi.org/10.1016/j.mineng.2004.03.002

Chow, M. F., Bahruddin, A. S., & Chua, K. H. (2023). Assessing the Efficiency of Green Absorbent in Treating Nutrients and Heavy Metal in Wastewater. Sustainability, 15(16), 12257. https://doi.org/10.3390/su151612257

Dack, K., Fell, M., Taylor, C. M., Havdahl, A., & Lewis, S. J. (2022). Prenatal mercury exposure and neurodevelopment up to the age of 5 years: A systematic review. *International Journal of Environmental Research and Public Health*, 19(4), 1976. https://doi.org/10.3390/ijerph19041976

David, M. K., Okoro, U. C., Akpomie, K. G., Okey, C., & Oluwasola, H. O. (2020). Thermal and hydrothermal alkaline modification of kaolin for the adsorptive removal of lead (II) ions from aqueous solution. SN Applied Sciences, 2, 1-13. https://doi.org/10.1007/s42452-020-2621-7

Ding, M., Su, H., Yang, K., Li, Y., Li, F., & Xue, B. (2021). Preparation and characterization of an aluminosilicate material with layer expansion structure. *Applied Clay Science*, 211, 106179. https://doi.org/10.1016/j.clay.2021.106179

do Nascimento, F. H., de Souza Costa, D. M., & Masini, J. C. (2016). Evaluation of thiol-modified vermiculite for removal of Hg(II) from aqueous solutions. Applied Clay Science, 124–125, 227–235. https://doi.org/10.1016/j.clay.2016.02.017

Edelstein, M., & Ben-Hur, M. (2018). Heavy metals and metalloids: Sources, risks and strategies to reduce their accumulation in horticultural crops. *Scientia Horticulturae*, *234*, 431-444. https://doi.org/10.1016/j.scienta.2017.12.039

Edelstein, M., & Ben-Hur, M. (2018). Heavy metals and metalloids: Sources, risks and strategies to reduce their accumulation in horticultural crops. *Scientia Horticulturae*, *234*, 431-444. https://doi.org/10.1016/j.scienta.2017.12.039

Fayazi, M. (2020). Removal of mercury (II) from wastewater using a new and effective composite: sulfur-coated magnetic carbon nanotubes. *Environmental science and pollution research*, *27*(11), 12270-12279. https://doi.org/10.1007/s11356-020-07843-z

Flagma.kz. (n.d.). Activated carbon products. Retrieved February 28, 2023, from https://flagma.kz/en/products/activated-carbon/q=%D1%83%D0%B3%D0%BE%D0%BB%D1%8C/

Freundlich, H. (1907). Über die adsorption in lösungen. *Zeitschrift für physikalische Chemie*, *57*(1), 385-470.

Fu, K., Liu, X., Lv, C., Luo, J., Sun, M., Luo, S., & Crittenden, J. C. (2022). Superselective Hg (II) removal from water using a thiol-laced MOF-based sponge monolith: performance and mechanism. *Environmental Science & Technology*, *56*(4), 2677-2688. https://doi.org/10.1021/acs.est.1c07480

Genchi, G., Sinicropi, M. S., Carocci, A., Lauria, G., & Catalano, A. (2017). Mercury exposure and heart diseases. *International journal of environmental research and public health*, *14*(1), 74. https://doi.org/10.3390/ijerph14010074

Goyanna, F. A. A., Fernandes, M. B., da Silva, G. B., & de Lacerda, L. D. (2023). Mercury in oceanic upper trophic level sharks and bony fishes-A systematic review. Environmental Pollution, 318, 120821. https://doi.org/10.1016/j.envpol.2022.120821

Guney, M., Akimzhanova, Z., Kumisbek, A., Beisova, K., Kismelyeva, S., Satayeva, A., ... & Karaca, F. (2020). Mercury (HG) contaminated sites in kazakhstan: Review of current cases and site remediation responses. International Journal of Environmental Research and Public Health, 17(23), 8936. https://doi.org/10.3390/ijerph17238936

Hua, K., Xu, X., Luo, Z., Fang, D., Bao, R., & Yi, J. (2020). Effective removal of mercury ions in aqueous solutions: A review. Current Nanoscience, 16(3), 363-375. https://doi.org/10.2174/1573413715666190112110659

Huang, Y., Gong, Y., Tang, J., & Xia, S. (2019). Effective removal of inorganic mercury and methylmercury from aqueous solution using novel thiol-functionalized graphene oxide/Fe-Mn composite. Journal of Hazardous Materials, 366, 130–139. https://doi.org/10.1016/j.jhazmat.2018.11.074

Huang, Y., Huang, Y., Fang, L., Zhao, B., Zhang, Y., Zhu, Y., ... & Li, F. (2023). Interfacial chemistry of mercury on thiol-modified biochar and its implication for adsorbent engineering. *Chemical Engineering Journal*, *454*, 140310. https://doi.org/10.1016/j.cej.2022.140310

Huang, Y., Tang, J., Gai, L., Gong, Y., Guan, H., He, R., & Lyu, H. (2017). Different approaches for preparing a novel thiol-functionalized graphene oxide/Fe-Mn and its application for aqueous methylmercury removal. Chemical Engineering Journal, 319, 229–239. https://doi.org/10.1016/j.cej.2017.03.015

Inglezakis, V. J., Kudarova, A., Guney, A., Kinayat, N., & Tauanov, Z. (2023). Efficient mercury removal from water by using modified natural zeolites and comparison to commercial adsorbents. *Sustainable Chemistry and Pharmacy*, 32, 101017. https://doi.org/10.1016/j.scp.2023.101017

Islam, M. S., Vogler, R. J., Abdullah Al Hasnine, S. M., Hernández, S., Malekzadeh, N., Hoelen, T. P., ... & Bhattacharyya, D. (2020). Mercury removal from wastewater using cysteamine functionalized membranes. *ACS omega*, 5(35), 22255-22267. https://doi.org/10.1021/acsomega.0c02526

Jiménez-Bautista, K., Gascó, A., Ramos, D. R., Palomo, E., Muelas-Ramos, V., Canle, M., ... & Bahamonde, A. (2023). Solar-assisted photodegradation of pesticides over pellet-shaped TiO2-kaolin catalytic macrocomposites at semi-pilot-plant scale: Elucidation of photo-mechanisms and water matrix effect. *Journal of Cleaner Production*, *426*, 139203. https://doi.org/10.1016/j.jclepro.2023.139203

Jurgelane, I., & Locs, J. (2023). Activated carbon and clay pellets coated with hydroxyapatite for heavy metal removal: characterization, adsorption, and regeneration. Materials, 16(9), 3605. https://doi.org/10.3390/ma16093605

Kerdoun, M. A., Alouk, L., Rahmani, F. M., Henni, H. A., Dali, H., Kelai, E., & Belkhalfa, H. (2024). Mercury in four common fishes sold in Algeria and associated humans risk. Food Additives & Contaminants: Part B, 1-7. https://doi.org/10.1080/19393210.2024.2353709

Khan, R., Saxena, A., Shukla, S., Sekar, S., Senapathi, V., & Wu, J. (2021). Environmental contamination by heavy metals and associated human health risk assessment: a case study of surface water in Gomti River Basin, India. Environmental Science and Pollution Research, 28(40), 56105-56116. https://doi.org/10.1007/s11356-021-14592-0

Kumar, S., Sharma, A., & Sedha, S. (2022). Occupational and environmental mercury exposure and human reproductive health-a review. *Journal of the Turkish German Gynecological Association*, 23(3), 199. https://doi.org/10.4274/jtgga.galenos.2022.2022-2-6

Langmuir, I. (1918). The adsorption of gases on plane surfaces of glass, mica and platinum. Journal of the American Chemical society, 40(9), 1361-1403.

Lenarda, M., Storaro, L., Talon, A., Moretti, E., & Riello, P. (2007). Solid acid catalysts from clays: Preparation of mesoporous catalysts by chemical activation of metakaolin under acid conditions. *Journal of colloid and interface science*, 311(2), 537-543. https://doi.org/10.1016/j.jcis.2007.03.015. 67

Li, F., Ma, C., & Zhang, P. (2020). Mercury deposition, climate change and anthropogenic activities: A review. *Frontiers in Earth Science*, *8*, 316. https://doi.org/10.3389/feart.2020.00316

Li, H., Chi, Z., & Li, J. (2015). Application of ion exchange and chemical precipitation process for the treatment of acid-dissolution water of chromium sludge. Desalination and Water Treatment, 53(1), 206-213. https://doi.org/10.1080/19443994.2013.837006

Li, S., Cooke, R. A., Wang, L., Ma, F., & Bhattarai, R. (2017). Characterization of fly ash ceramic pellet for phosphorus removal. Journal of environmental management, 189, 67-74. https://doi.org/10.1016/j.jenvman.2016.12.042

Lin, Z., Pan, Z., Zhao, Y., Qian, L., Shen, J., Xia, K., Guo, Y., & Qu, Z. (2020). Removal of Hg2+ with polypyrrole-functionalized Fe3O4/kaolin: Synthesis, performance and optimization with response surface methodology. Nanomaterials, 10(7), 1–23. https://doi.org/10.3390/nano10071370

Liu, Y., Xue, F., Wang, T., Wang, Q., & Pan, W. P. (2023). Three-dimensional ordered zeolite templated carbon with covalent sulfur for efficient removal of elemental mercury: Experimental study and molecular dynamic simulation. *Fuel Processing Technology*, 239, 107540. https://doi.org/10.1016/j.fuproc.2022.107540

Merck. (n.d.). Zeolite, powder (Product No. 96096). Sigma-Aldrich. https://www.sigmaaldrich.com/KZ/en/product/sigma/96096

Merck. (n.d.). Kaolin for analysis EMSURE® ISO (Product No. 104440). Sigma-Aldrich. https://www.sigmaaldrich.com/KZ/en/product/mm/104440

Mouni, L., Belkhiri, L., Bollinger, J. C., Bouzaza, A., Assadi, A., Tirri, A., Dahmoune, F., Madani, K., & Remini, H. (2018). Removal of Methylene Blue from aqueous solutions by adsorption on Kaolin: Kinetic and equilibrium studies. Applied Clay Science, 153, 38–45. https://doi.org/10.1016/j.clay.2017.11.034

Moussout, H., Ahlafi, H., Aazza, M., & Maghat, H. (2018). Critical of linear and nonlinear equations of pseudo-first order and pseudo-second order kinetic models. *Karbala International Journal of Modern Science*, *4*(2), 244-254. https://doi.org/10.1016/j.kijoms.2018.04.001

Mustapha, S., Ndamitso, M. M., Abdulkareem, A. S., Tijani, J. O., Mohammed, A. K., & Shuaib, D. T. (2019). Potential of using kaolin as a natural adsorbent for the removal of pollutants from tannery wastewater. Heliyon, 5(11). https://doi.org/10.1016/j.heliyon.2019.e02923

Mustapha, S., Tijani, J. O., Ndamitso, M. M., Abdulkareem, A. S., Shuaib, D. T., & Mohammed, A. K. (2021). Adsorptive removal of pollutants from industrial wastewater using mesoporous kaolin and kaolin/TiO2 nanoadsorbents. Environmental Nanotechnology, Monitoring and Management, 15. https://doi.org/10.1016/j.enmm.2020.100414

Nayak, S. (2021). Water purification: Removal of Heavy metals Using Metal-Organic Frameworks (MOFs). *Metal-Organic Frameworks in Biomedical and Environmental Field*, 239-268. https://doi.org/10.1007/978-3-030-63380-6_7

Ogarekpe, N. M., Nnaji, C. C., Oyebode, O. J., Ekpenyong, M. G., Ofem, O. I., Tenebe, I. T., & Asitok, A. D. (2023). Groundwater quality index and potential human health risk assessment of heavy metals in water: A case study of Calabar metropolis, Nigeria. Environmental Nanotechnology, Monitoring & Management, 19, 100780. https://doi.org/10.1016/j.enmm.2023.100780

Park, J. H., Wang, J. J., Zhou, B., Mikhael, J. E., & DeLaune, R. D. (2019). Removing mercury from aqueous solution using sulfurized biochar and associated mechanisms. *Environmental pollution*, 244, 627-635. https://doi.org/10.1016/j.envpol.2018.10.069

Pei, P., Sun, T., Xu, Y., & Sun, Y. (2022). Using thiol-functionalized montmorillonites for chemically immobilizing Hg in contaminated water and soil: A comparative study of intercalation and grafting functionalization. Applied Clay Science, 216, 106381. https://doi.org/10.1016/j.clay.2021.106381

Pei, P., Xu, Y., Wang, L., Liang, X., & Sun, Y. (2022). Thiol-functionalized montmorillonite prepared by one-step mechanochemical grafting and its adsorption performance for

mercury and methylmercury. Science of The Total Environment, 806, 150510. https://doi.org/10.1016/j.scitotenv.2021.150510

Qasem, N. A., Mohammed, R. H., & Lawal, D. U. (2021). Removal of heavy metal ions from wastewater: A comprehensive and critical review. Npj Clean Water, 4(1), 1-15. https://doi.org/10.1038/s41545-021-00127-0

Rao, M. M., Reddy, D. K., Venkateswarlu, P., & Seshaiah, K. (2009). Removal of mercury from aqueous solutions using activated carbon prepared from agricultural by-product/waste. *Journal of environmental management*, 90(1), 634-643. https://doi.org/10.1016/j.jenvman.2007.12.019

Roa, K., Trejo, F., & Castro, H. (2023). Application of porous geopolymer composite 1 based on metakaolin and activated carbon for removal of Hg2+ from aqueous solution. Journal of applied research and technology, 21(5), 796-807. https://doi.org/10.22201/icat.24486736e.2023.21.5.1702

Santos, I. D. S. D., Bao, S. X., & Musah, B. I. (2022). Metakaolin-based geopolymer for mercury removal from model wastewater. *Water Environment Research*, 94(8), e10779. https://doi.org/10.1002/wer.10779

Satu.kz. (n.d.). TOO Himiya Tehnologiya. Retrieved February 28, 2023, from https://satu.kz/c19704-too-himiya-tehnologiya.html

Simonin, J. P. (2016). On the comparison of pseudo-first order and pseudo-second order rate laws in the modeling of adsorption kinetics. *Chemical Engineering Journal*, *300*, 254-263. https://doi.org/10.1016/j.cej.2016.04.079

Sing, K. S. (1985). Reporting physisorption data for gas/solid systems with special reference to the determination of surface area and porosity (Recommendations 1984). *Pure and applied chemistry*, *57*(4), 603-619.

Tang, S. H., & Zaini, M. A. A. (2020). Development of activated carbon pellets using a facile lowcost binder for effective malachite green dye removal. Journal of Cleaner Production, 253, 119970. https://doi.org/10.1016/j.jclepro.2020.119970

Teng, H., & Altaf, A. R. (2022). Elemental mercury (Hg0) emission, hazards, and control: A brief review. Journal of Hazardous Materials Advances, 5, 100049. https://doi.org/10.1016/j.hazadv.2022.100049

Vareda, J. P., Valente, A. J., & Durães, L. (2019). Assessment of heavy metal pollution from anthropogenic activities and remediation strategies: A review. Journal of environmental management, 246, 101-118. https://doi.org/10.1016/j.jenvman.2019.05.126

Wang, H., Li, C., Peng, Z., & Zhang, S. (2011). Characterization and thermal behavior of kaolin. *Journal of Thermal Analysis and Calorimetry*, *105*(1), 157-160. https://doi.org/10.1007/s10973-011-1385-0

Wang, Y., He, T., Yin, D., Han, Y., Zhou, X., Zhang, G., & Tian, X. (2020). Modified clay mineral: A method for the remediation of the mercury-polluted paddy soil. *Ecotoxicology and Environmental Safety*, 204, 111121. https://doi.org/10.1016/j.ecoenv.2020.111121

Wang, Y., Li, S., & Yang, H. (2019). In situ stabilization of some mercury-containing soils using organically modified montmorillonite loading by thiol-based material. Journal of Soils and Sediments, 19, 1767-1774. https://doi.org/10.1007/s11368-018-2150-9

Xiang, H., Min, X., Tang, C. J., Sillanpää, M., & Zhao, F. (2022). Recent advances in membrane filtration for heavy metal removal from wastewater: A mini review. Journal of Water Process Engineering, 49, 103023. https://doi.org/10.1016/j.jwpe.2022.103023

Xiao, B. K. M. T., & Thomas, K. M. (2004). Competitive adsorption of aqueous metal ions on an oxidized nanoporous activated carbon. Langmuir, 20(11), 4566-4578. https://doi.org/10.1021/la049712j

Xu, Y., Zhang, S., Zhao, Y., Yang, J., Shen, S., Zhang, G., ... & Zheng, X. (2022). Efficient removal of Hg2+ by L-cysteine and polypyrrole-functionalized magnetic kaolin: condition optimization, model fitting and mechanism. Research on Chemical Intermediates, 48(10), 4287-4311. https://doi.org/10.1007/s11164-022-04794-7

Yılmaz, Ş., Şahan, T., & Karabakan, A. (2017). Response surface approach for optimization of Hg (II) adsorption by 3-mercaptopropyl trimethoxysilane-modified kaolin minerals from aqueous solution. Korean Journal of Chemical Engineering, 34, 2225-2235. https://doi.org/10.1007/s11814-017-0116-z

Yu, G., Lu, Y., Guo, J., Patel, M., Bafana, A., Wang, X., ... & Wujcik, E. K. (2018). Carbon nanotubes, graphene, and their derivatives for heavy metal removal. *Advanced Composites and Hybrid Materials*, *1*, 56-78. https://doi.org/10.1007/s42114-017-0004-3

Zeng, Q., Wang, H., Ran, H., Wu, J., & Yang, K. (2023). Mercury removal performance and mechanism of biochar co-modified with HNO3 and NH4Br under oxy-combustion atmosphere. *Energy Sources*, Part A: Recovery, Utilization, and Environmental Effects, 45(3), 8167-8182. https://doi.org/10.1080/15567036.2023.2226100

Zhang, Q., Yan, Z., Ouyang, J., Zhang, Y., Yang, H., & Chen, D. (2018). Chemically modified kaolinite nanolayers for the removal of organic pollutants. Applied Clay Science, 157, 283–290. https://doi.org/10.1016/j.clay.2018.03.009

Zhao, C., Zhou, J., Yan, Y., Yang, L., Xing, G., Li, H., ... & Zheng, H. (2021). Application of coagulation/flocculation in oily wastewater treatment: A review. Science of The Total Environment, 765, 142795. https://doi.org/10.1016/j.scitotenv.2020.142795